

# Quantum Circuit Optimization with AlphaTensor

Francisco J. R. Ruiz<sup>\*,1</sup>      Tuomas Laakkonen<sup>\*,2</sup>      Johannes Bausch<sup>1</sup>  
Matej Balog<sup>1</sup>      Mohammadamin Barekatin<sup>1</sup>      Francisco J. H. Heras<sup>1</sup>  
Alexander Novikov<sup>1</sup>      Nathan Fitzpatrick<sup>3</sup>      Bernardino Romera-Paredes<sup>1</sup>  
John van de Wetering<sup>4</sup>      Alhussein Fawzi<sup>1</sup>      Konstantinos Meichanetzidis<sup>2</sup>  
Pushmeet Kohli<sup>1</sup>

<sup>1</sup> Google DeepMind, 6-8 Handyside Street, London N1C 4UZ, UK

<sup>2</sup> Quantinuum, 17 Beaumont Street, Oxford OX1 2NA, UK

<sup>3</sup> Quantinuum, Terrington House, 13–15 Hills Road, Cambridge CB2 1NL, UK

<sup>4</sup> Informatics Institute, University of Amsterdam, 1098 XH Amsterdam, NL

## Abstract

A key challenge in realizing fault-tolerant quantum computers is circuit optimization. Focusing on the most expensive gates in fault-tolerant quantum computation (namely, the T gates), we address the problem of T-count optimization, i.e., minimizing the number of T gates that are needed to implement a given circuit. To achieve this, we develop AlphaTensor-Quantum, a method based on deep reinforcement learning that exploits the relationship between optimizing T-count and tensor decomposition. Unlike existing methods for T-count optimization, AlphaTensor-Quantum can incorporate domain-specific knowledge about quantum computation and leverage *gadgets*, which significantly reduces the T-count of the optimized circuits. AlphaTensor-Quantum outperforms the existing methods for T-count optimization on a set of arithmetic benchmarks (even when compared without making use of gadgets). Remarkably, it discovers an efficient algorithm akin to Karatsuba’s method for multiplication in finite fields. AlphaTensor-Quantum also finds the best human-designed solutions for relevant arithmetic computations used in Shor’s algorithm and for quantum chemistry simulation, thus demonstrating it can save hundreds of hours of research by optimizing relevant quantum circuits in a fully automated way.

## 1 Introduction

Quantum computation presents a fundamentally new approach to solving computational problems. Since its inception [1, 2], many potential applications in various fields have been proposed, including cryptography [3], drug discovery [4], and materials science and high energy physics [5]. Yet, fault-tolerant quantum computation introduce some expensive components that have a significant impact on the overall runtime and resource cost [6, 7]; thus it is important to minimize the use of these components in order to enable the execution of large computations that address these real-world problems.

---

\*Equal contributors.

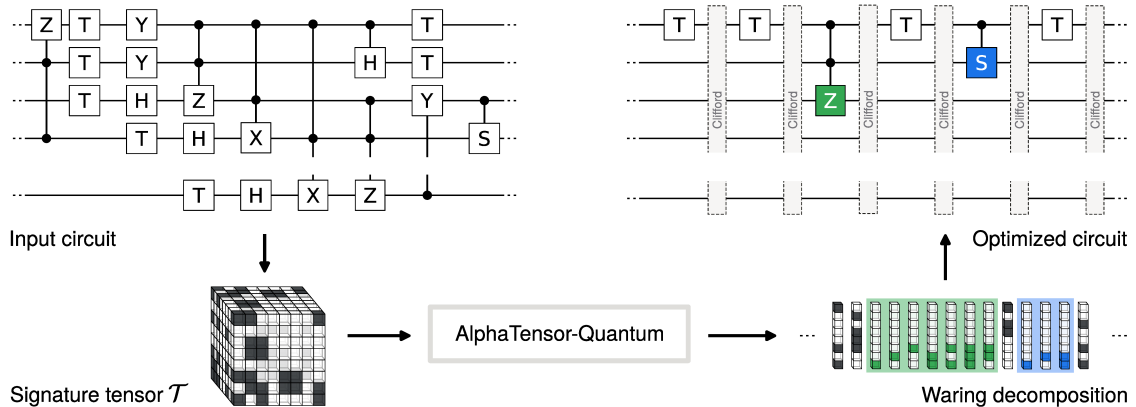


**Figure 1:** Pipeline of AlphaTensor-Quantum. We first extract the non-Clifford components of an input circuit and represent them as a symmetric *signature tensor*  $\mathcal{T}$ , a binary tensor depicted as a cube of solid and transparent blocks. We then use AlphaTensor-Quantum to find a low-rank Waring decomposition of that tensor, that is, a set of factors (displayed as columns of blocks) that can be mapped back into an optimized quantum circuit with reduced T-count. In general, there is a one-to-one correspondence between factors and T gates, but AlphaTensor-Quantum can also group factors into *gadgets* (highlighted in green and blue)—constructions that can be equivalently implemented with fewer T gates than the sum of the factors.

To be able to implement any quantum algorithm, universal quantum computers require a combination of two types of quantum gates: Clifford (e.g., Hadamard or CNOT) and non-Clifford gates (e.g., the T gate). Non-Clifford gates are required to achieve universality [8]; indeed, a quantum algorithm implemented using Clifford gates alone can be simulated on a classical computer efficiently, i.e., in polynomial time (Gottesman–Knill theorem [9]). Unfortunately, non-Clifford gates are the expensive components, as they are notoriously harder to implement than Clifford gates. This is because fault-tolerant quantum computation requires error correction schemes [10, 11], whose implementation requires distilling magic states [6], a process with high spacetime cost (qubit-seconds) [12]. For example, the spacetime cost of the T gate is about two orders of magnitude larger than the cost of a CNOT operation between two adjacent qubits [8]. Consequently, the cost of a quantum algorithm in the fault-tolerant era is arguably dominated by the cost of implementing the non-Clifford gates.

In this paper, we focus on the problem of T-count optimization, i.e., minimizing the number of T gates of quantum algorithms. T-count optimization is an NP-hard problem [13] that has been addressed in the literature using different approaches [14–23]. Like most of these works, and for the reasons laid out before, we consider the T-count as the *sole* metric of complexity of a quantum circuit.

With that aim, we first transform the problem into an instance of tensor decomposition, exploiting the relationship between T-count optimization and finding the symmetric tensor rank [16, 18]. We develop *AlphaTensor-Quantum*, an extension of AlphaTensor [24], a method that finds low-rank tensor decompositions using deep reinforcement learning (RL). AlphaTensor-Quantum tackles the problem from the tensor decomposition point of view and is able to find efficient algorithm implementations with low T-count. The approach is illustrated in Figure 1.

AlphaTensor-Quantum addresses three main challenges that go beyond the capabilities of AlphaTensor [24] when applied on this problem. First, we need to optimize the *symmetric* tensor rank, as opposed to the standard notion of tensor rank. Second, the approach must extend to *large tensor sizes*, since the size of the tensor corresponds directly to the number of qubits in the circuit to be optimized. Third, AlphaTensor cannot leverage domain knowledge that falls outside of the tensor decomposition framework. AlphaTensor-Quantum addresses these three challenges. First, it modifies the RL environment and actions to provide symmetric decompositions (called *Waring decompositions*) of the tensor; this has the beneficial side effect of reducing the action search space. Second, it scales up to larger tensors due to its innovative neural network architecture featuring *symmetrization layers*. Third, it incorporates domain knowledge by leveraging so-called *gadgets* (constructions that can save T gates by using auxiliary ancilla qubits); this is achieved through an efficient procedure embedded in the RL environment that exploits the Toffoli gadget [25] and the controlled S (CS) gadget [26].

We show that AlphaTensor-Quantum is a powerful method for finding efficient quantum circuits. On a benchmark of arithmetic primitives, AlphaTensor-Quantum outperforms all existing methods for T-count optimization, especially when allowed to leverage domain knowledge. For the relevant operation of multiplication in finite fields, which has applications in cryptography [27], AlphaTensor-Quantum finds an efficient quantum algorithm with the same complexity as the *classical* Karatsuba’s method [28]. As quantum computations are reversible by nature, naive translations of classical algorithms commonly introduce overhead [29, 30]. AlphaTensor-Quantum thus finds the most efficient quantum algorithm for multiplication on finite fields reported to date. We also optimize quantum primitives for other relevant problems, ranging from arithmetic computations used, e.g., in Shor’s algorithm [31], to Hamiltonian simulation in quantum chemistry, e.g., FeMoco simulation [32, 33]. Here, AlphaTensor-Quantum recovers the best known hand-designed solutions, demonstrating it can effectively optimize circuits of interest in a fully automated way. We envision this approach can significantly accelerate discoveries in quantum computation as it saves the numerous hours of research invested in the design of optimized circuits.

These results show that AlphaTensor-Quantum can effectively exploit the domain knowledge that is provided in the form of gadgets and state-of-the-art magic state factories [8], finding constructions that are optimal for the chosen metrics of interest. Because of its flexibility, AlphaTensor-Quantum can be readily extended in multiple ways, e.g., by considering different complexity metrics (other than the T-count), or by incorporating new domain knowledge. Thus, we expect that AlphaTensor-Quantum will become instrumental for automatic circuit optimization with new advancements in quantum computing.

## 2 AlphaTensor-Quantum for T-count Optimization

We describe AlphaTensor-Quantum, an RL agent to optimize the T-count of quantum circuits. It relies on the relation between T-count optimization and tensor decomposition (see Figure 1), which we briefly review next.

**Quantum gates.** Quantum computers work with *qubits*. The state of a qubit is representable as a L2-normalized vector in  $\mathbb{C}^2$ , typically denoted with the *bra-ket* notation as  $|\psi\rangle$ , with the basis vectors being  $|0\rangle$  and  $|1\rangle$ . An  $N$ -qubit state is represented by a normalized vector in  $\mathbb{C}^{2^N}$ . Quantum circuits perform linear operations over a quantum state that preserve the normalization, thus they can be represented by *unitary matrices*. Quantum circuits are implemented by *quantum gates*.

Quantum operator	#Qubits	Gate symbol	Unitary matrix
Controlled NOT (CNOT)	2		$\begin{pmatrix} 1 & 0 & 0 & 0 \\ 0 & 1 & 0 & 0 \\ 0 & 0 & 0 & 1 \\ 0 & 0 & 1 & 0 \end{pmatrix}$
Controlled S (CS)	2		$\begin{pmatrix} 1 & 0 & 0 & 0 \\ 0 & 1 & 0 & 0 \\ 0 & 0 & 1 & 0 \\ 0 & 0 & 0 & i \end{pmatrix}$
Controlled Z (CZ)	2		$\begin{pmatrix} 1 & 0 & 0 & 0 \\ 0 & 1 & 0 & 0 \\ 0 & 0 & 1 & 0 \\ 0 & 0 & 0 & -1 \end{pmatrix}$
Controlled controlled Z (CCZ)	3		$\begin{pmatrix} 1 & 0 & 0 & 0 & 0 & 0 & 0 & 0 \\ 0 & 1 & 0 & 0 & 0 & 0 & 0 & 0 \\ 0 & 0 & 1 & 0 & 0 & 0 & 0 & 0 \\ 0 & 0 & 0 & 1 & 0 & 0 & 0 & 0 \\ 0 & 0 & 0 & 0 & 1 & 0 & 0 & 0 \\ 0 & 0 & 0 & 0 & 0 & 1 & 0 & 0 \\ 0 & 0 & 0 & 0 & 0 & 0 & 1 & 0 \\ 0 & 0 & 0 & 0 & 0 & 0 & 0 & -1 \end{pmatrix}$
Toffoli (Controlled CNOT)	3		$\begin{pmatrix} 1 & 0 & 0 & 0 & 0 & 0 & 0 & 0 \\ 0 & 1 & 0 & 0 & 0 & 0 & 0 & 0 \\ 0 & 0 & 1 & 0 & 0 & 0 & 0 & 0 \\ 0 & 0 & 0 & 1 & 0 & 0 & 0 & 0 \\ 0 & 0 & 0 & 0 & 1 & 0 & 0 & 0 \\ 0 & 0 & 0 & 0 & 0 & 1 & 0 & 0 \\ 0 & 0 & 0 & 0 & 0 & 0 & 1 & 0 \\ 0 & 0 & 0 & 0 & 0 & 0 & 0 & 1 \end{pmatrix}$

**Table 1:** Common controlled gates used in quantum computing, along with their symbols and unitary matrices.

Following convention, we focus on the Clifford+T gate set because it is the leading candidate for fault-tolerant implementation and it is approximately universal, meaning that any unitary matrix can be approximated arbitrarily well by a circuit consisting of these gates. In particular, we consider the following gate set: Hadamard (H) and controlled NOT (CNOT), which are Clifford gates, and T gates, given by the unitary matrices

$$T = \begin{pmatrix} 1 & 0 \\ 0 & e^{i\pi/4} \end{pmatrix}, \quad H = \frac{1}{\sqrt{2}} \begin{pmatrix} 1 & 1 \\ 1 & -1 \end{pmatrix}, \quad \text{and} \quad CNOT = \begin{pmatrix} 1 & 0 & 0 & 0 \\ 0 & 1 & 0 & 0 \\ 0 & 0 & 0 & 1 \\ 0 & 0 & 1 & 0 \end{pmatrix}.$$

For convenience, we also define the following Clifford gates:

$$S = T^2, \quad Z = S^2, \quad X = \begin{pmatrix} 0 & 1 \\ 1 & 0 \end{pmatrix}, \quad \text{and} \quad Y = \begin{pmatrix} 0 & -i \\ i & 0 \end{pmatrix}.$$

Each of these gates, except the CNOT, acts on a single qubit. The T, S, and Z gates perform phase operations, e.g., for a quantum state  $|x\rangle$  with  $x \in \{0, 1\}$ , we have  $T|x\rangle = e^{i\frac{\pi}{4}x}|x\rangle$ . The CNOT acts on two qubits: it flips the second qubit if the first qubit is in the  $|1\rangle$  state, i.e.,  $CNOT|x, y\rangle = |x, x \oplus y\rangle$ , where ‘ $\oplus$ ’ denotes the XOR operation. Controlled gates like the CNOT enable quantum entanglement; these gates are summarized in Table 1. For instance, the controlled CNOT, or Toffoli gate, acts on three qubits and applies the operation  $Tof|x, y, z\rangle = |x, y, z \oplus (xy)\rangle$ .

Quantum gates can be composed to implement arbitrary unitary operations: serial composition corresponds to matrix multiplication, and parallel composition corresponds to Kronecker product.

**Signature tensor.** Given a circuit composed of CNOT and T gates alone, we can encode the information about the non-Clifford components into a symmetric *signature tensor*  $\mathcal{T} \in \{0, 1\}^{N \times N \times N}$ , with  $N$  being the number of qubits. Indeed, two CNOT + T circuits implement the same unitary matrix, up to Clifford gates, if and only if they have the same signature tensor [16, 18] (see Section 5.1).

To optimize the T-count of a circuit, we first find its representation in terms of the signature tensor  $\mathcal{T}$ . When the circuit has gates other than CNOT and T gates alone, to obtain the signature tensor we first split the circuit into two parts—one that consists only of Clifford gates, and a diagonal part that contains only CNOT and T gates. We do this using the techniques of Heyfron and Campbell [16] in combination with the algorithm by Vandaele et al. [34] (see Figure 3 for an example and Appendix C.1 for more details).

After that, we obtain  $\mathcal{T}$  by first mapping each T gate to a vector  $u^{(r)} \in \{0, 1\}^N$ , which is a straightforward step [35], and then constructing the tensor from the *Waring decomposition* (a symmetric form of the tensor rank decomposition) given by these vectors, i.e.,

$$\mathcal{T} = \sum_{r=1}^R u^{(r)} \otimes u^{(r)} \otimes u^{(r)},$$

where  $R$  is the number of T gates, ‘ $\otimes$ ’ denotes the outer product, and the additions are under modulo 2.

Crucially, any *alternative* Waring decomposition of  $\mathcal{T}$  can *also* be mapped to a quantum circuit, as each vector  $u^{(r)}$  corresponds one-to-one to a T gate. The resulting circuit is equivalent to the original one up to Clifford operations [18], albeit with a different number of T gates—according to the number of factors  $R$  in the decomposition. Hence, we recast the problem of T-count optimization as finding low-rank decompositions of  $\mathcal{T}$ .

**TensorGame.** AlphaTensor-Quantum is an RL-based tensor factorization approach that finds low-rank Waring decompositions of tensors. It builds upon AlphaTensor [24], which uses deep RL to find low-rank decompositions of 3-dimensional tensors. AlphaTensor-Quantum recasts the problem of tensor decomposition into a single-player game, called *TensorGame*, in which at each step  $s$  the player observes the *game state*, consisting of a tensor  $\mathcal{T}^{(s)}$  and all the past played actions (initially, the tensor  $\mathcal{T}^{(1)}$  is set to the signature tensor of interest  $\mathcal{T}$ , and there are no past actions). At step  $s$ , the player selects an *action* consisting of a vector (or factor)  $u^{(s)} \in \{0, 1\}^N$ . Choosing an action affects the game state: the tensor  $\mathcal{T}^{(s+1)} = \mathcal{T}^{(s)} - u^{(s)} \otimes u^{(s)} \otimes u^{(s)}$ , and  $u^{(s)}$  is included as the last played action. The goal of TensorGame is to reach the all-zero tensor in as few moves as possible. The game ends after  $S$  moves if that is the case and, by construction, the played actions form a rank- $S$  Waring decomposition of the signature tensor, since  $\mathcal{T} = \sum_{s=1}^S u^{(s)} \otimes u^{(s)} \otimes u^{(s)}$ . (The game also ends after a user-specified maximum number of moves to avoid infinitely long games, in which case the game is declared “unsuccessful” as it did not find a decomposition of the tensor.) To encourage the RL agent to find low-rank decompositions or, equivalently, circuits with lower T-count, games are penalized based on the number of moves taken to reach the all-zero tensor (with an additional penalty for unsuccessful games): every played move incurs a reward of  $-1$ .

In AlphaTensor-Quantum, each action consists of a single factor  $u^{(s)}$ . This represents a significant advantage over standard AlphaTensor (where actions consist of factor triplets), because for a fixed tensor size  $N$ ,

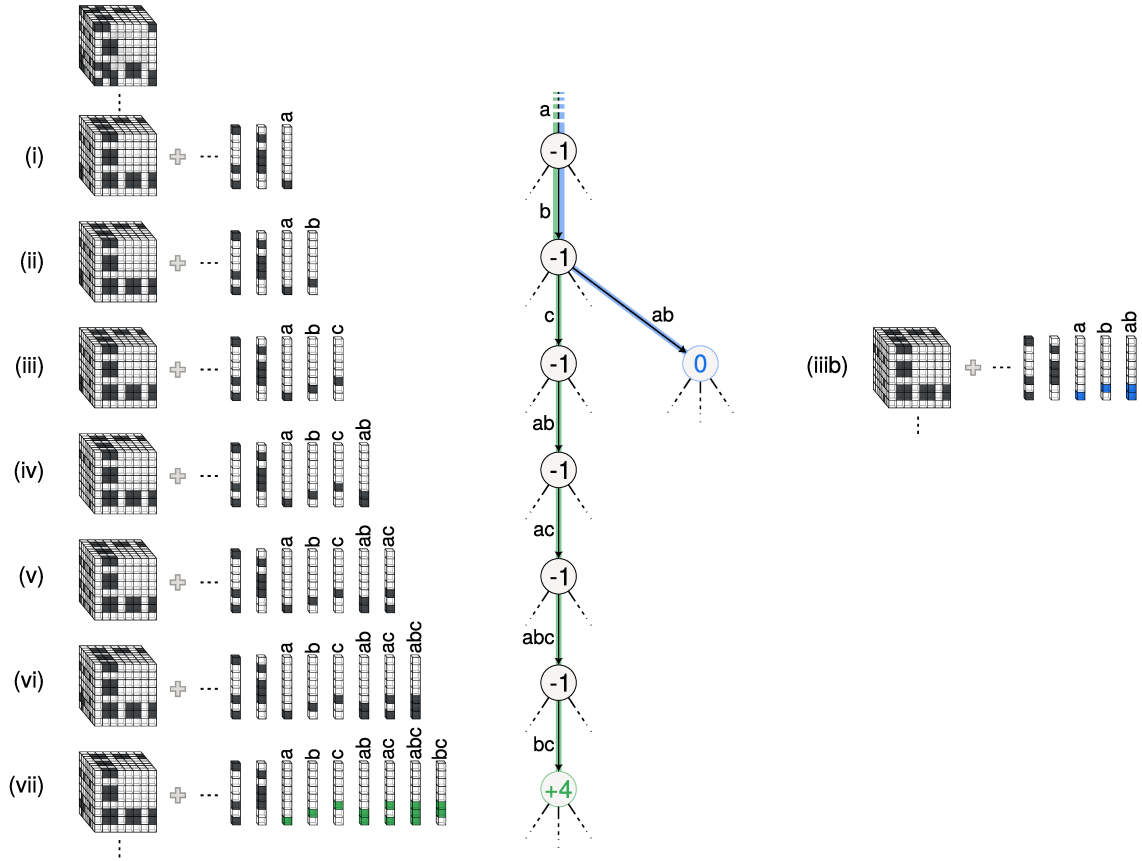


**Figure 2:** Illustration of gadgetization in TensorGame. Nodes in the tree correspond to states, and the number in each node is the immediate reward associated to the action leading to that node. In state (i), the last played action is labeled “a”, and state (ii) is reached after playing another action (labeled “b”). From state (ii), playing action “c” leads to state (iii), incurring an additional  $-1$  reward. If action “ab” is played instead from state (ii), the reward leading to state (iiiib) is 0 because the move completes a CS gadget (blue path). Similarly, the sequence of moves in the green path completes a Toffoli gadget, and thus the immediate reward in state (vii) is  $+4$  so that the last seven actions jointly receive a reward of  $-2$  (see Section 5.2 for details on the gadgetization patterns). With its ability to plan, from state (i) the agent may decide to play actions in the green or blue paths and benefit from the adjusted rewards, or to play other actions that are not part of a gadget (black dashed paths). In this way, AlphaTensor-Quantum can automatically find trade-offs between playing actions that are part of a gadget and actions that are not.

the action space reduces from  $2^{3N}$  to  $2^N$ . This is one of the key properties that allows AlphaTensor-Quantum to scale up to tensors larger than the ones considered by Fawzi et al. [24]; we consider tensors of size up to  $N = 72$  in Section 3.

**Gadgets.** In contrast to other state-of-the-art T-count optimization approaches, AlphaTensor-Quantum can leverage *gadgetization* techniques to find more efficient constructions. In this context, a gadget is an alternative implementation of a quantum gate that reduces the number of T gates at the cost of introducing additional (ancilla) qubits and operations such as Clifford gates and measurement-based corrections. (These extra qubits do not represent a significant limitation in practice, as they can be reused throughout the circuit.)

We consider two such gadgets. First, the Toffoli gate, a quantum gate that needs at least seven T gates [15] to implement without ancillae. The Toffoli gate admits a gadget to implement it using four T gates [25], or when considering a state-of-the-art magic state factory [8], a gadget to implement it at a cost equivalent to that of two T gates. Second, the CS gate, which can be built with a cost equivalent to that of two T gates due to the magic state factory, instead of the three T gates of its direct implementation [26, Appendix A.3].

Although the gadgetization techniques fall outside of the tensor decomposition framework, AlphaTensor-Quantum incorporates them into TensorGame as follows. Every time that an action is played, we check whether it completes a Toffoli when combined with the six previous actions, a CS gate when combined with the two previous actions, or none of them. (These checks are up to Clifford operations and they simply involve finding linear dependencies among the factors; see Section 5.2 and appendix C.3 for details.) If it completes a Toffoli, we assign a positive reward, so that the seven actions jointly incur a reward of  $-2$  (corresponding to two T gates) as opposed to the reward of  $-7$  corresponding to the un-gadgetized implementation. If it completes a CS, we adjust the reward so that the three actions jointly incur a reward of  $-2$ . See Figure 2 for an illustration of a TensorGame with gadgetization.

Other than the reward signal, AlphaTensor-Quantum has no further information about the gadgets. It learns to recognize and exploit those patterns of actions from the data, and it finds good trade-offs between playing actions that are part of a gadget and actions that are not.

## 3 Results

Section 3.1 demonstrates the effectiveness of AlphaTensor-Quantum on a benchmark of circuits widely used in the literature of T-count optimization, and Section 3.2 shows applications of AlphaTensor-Quantum in different domains.

### 3.1 Benchmark Circuits

We consider a benchmark set of quantum circuits originally proposed by Amy et al. [14] and widely used in the literature of T-count optimization [16–18, 23]. We take the circuits from Amy [36] (we also include  $\text{GF}(2^2)$ -mult and  $\text{GF}(2^3)$ -mult for completeness; see Appendix D.1) and apply two versions of AlphaTensor-Quantum: the full approach that includes gadgetization, and an alternative agent that does not consider any gadgets. We report the resulting T-count for each approach in Table 2.

**Circuit compilation.** We apply a standard compilation technique [16, 23] with an improvement [34] (see Appendix C.1 for details and Figure 3 for an example). To make the circuits amenable to the tensor decomposition approach, we replace the Hadamard gates by extra ancilla qubits and Clifford gates (we refer to this as *Hadamard gadgetization* [16] to distinguish it from the gadgetization described in Section 2). For circuits exceeding 60 qubits after this process, we split them into smaller sub-circuits of fewer than 60 qubits each, and apply AlphaTensor-Quantum on each sub-circuit independently. We split the circuits at the boundaries corresponding to Hadamard gates via a random-greedy algorithm designed to minimize the number of splits (see Appendix C.2).

**Results.** In Table 2, we compare the results of the non-gadgetized version of AlphaTensor-Quantum against the best T-count reported in the literature [14, 16–19, 22, 23, 37, 38], as the baselines do not consider any gadgets either. For the circuits that did not require splitting, AlphaTensor-Quantum matches or outperforms all the existing T-count optimization methods. For all small circuits (at most 20 T gates), we confirmed with the Z3 theorem prover [39] that AlphaTensor-Quantum obtains the best possible T-count achievable with a tensor decomposition approach. For the circuits that exceed 60 qubits, AlphaTensor-Quantum outperforms the baselines for  $\text{Hamming}_{15}$  (high) and  $\text{Mod-Adder}_{1024}$ , but not for the others, likely due to the lack of optimality of the splitting technique.

When considering gadgets, AlphaTensor-Quantum leverages the Toffoli and CS gates to *further drastically reduce* the T-count. When compared against the original construction of the circuits, consisting mostly of Toffoli gates, AlphaTensor-Quantum reduces the T-count in all except two cases (likely due to the splitting). When compared against the baselines, AlphaTensor-Quantum reduces the T-count for all circuits except  $\text{Grover}_5$ . Remarkably, for the  $\text{GF}(2^m)$ -mult circuits, AlphaTensor-Quantum finds constructions with significantly smaller T-count than the baselines or the original constructions; we discuss this further in Section 3.2.

Circuit	#Qubits		T-count without gadgets		T-count with gadgets	
	Original	Compiled	Baselines	AlphaTensor-Quantum	Original	AlphaTensor-Quantum
8-bit adder	24	★	<b>129</b> [16]	139	114 (57Tof)	<b>94</b> (33Tof + 28T)
Barenco Toff <sub>3</sub>	5	8	13 [22, 23]	13*	8 (4Tof)	<b>4</b> (2Tof)
Barenco Toff <sub>4</sub>	7	14	24 [16, 22]	<b>23</b>	16 (8Tof)	<b>8</b> (4Tof)
Barenco Toff <sub>5</sub>	9	20	34 [16, 22]	<b>33</b>	24 (12Tof)	<b>12</b> (6Tof)
Barenco Toff <sub>10</sub>	19	50	84 [16]	<b>83</b>	64 (32Tof)	<b>32</b> (16Tof)
CSLA-MUX <sub>3</sub>	15	21	40 [22]	<b>39</b>	20 (10Tof)	<b>16</b> (8Tof)
CSUM-MUX <sub>9</sub>	30	42	72 [16, 19]	<b>71</b>	56 (28Tof)	<b>28</b> (14Tof)
GF(2 <sup>2</sup> )-mult	6	6	17 <sup>†</sup>	17*	8 (4Tof)	<b>6</b> (3Tof)
GF(2 <sup>3</sup> )-mult	9	9	31 <sup>†</sup>	<b>29</b>	18 (9Tof)	<b>12</b> (6Tof)
GF(2 <sup>4</sup> )-mult	12	12	47 [22]	<b>39</b>	32 (16Tof)	<b>18</b> (9Tof)
GF(2 <sup>5</sup> )-mult	15	15	84 [22]	<b>59</b>	50 (25Tof)	<b>26</b> (13Tof)
GF(2 <sup>6</sup> )-mult	18	18	118 [22]	<b>77</b>	72 (36Tof)	<b>36</b> (18Tof)
GF(2 <sup>7</sup> )-mult	21	21	167 [23]	<b>104</b>	98 (49Tof)	<b>44</b> (22Tof)
GF(2 <sup>8</sup> )-mult	24	24	214 [19]	<b>123</b>	128 (64Tof)	<b>58</b> (29Tof)
GF(2 <sup>9</sup> )-mult	27	27	295 [16]	<b>161</b>	162 (81Tof)	<b>70</b> (35Tof)
GF(2 <sup>10</sup> )-mult	30	30	350 [16]	<b>196</b>	200 (100Tof)	<b>92</b> (46Tof)
Grover <sub>5</sub>	9	★	<b>44</b> [16]	152	96 (48Tof)	<b>66</b> (27Tof + 12T)
Hamming <sub>15</sub> (high)	20	★	787 <sup>†</sup> (1010 [16])	<b>773</b>	702 (351Tof)	<b>440</b> (173Tof + 2CS + 90T)
Hamming <sub>15</sub> (low)	17	42	75 [16]	<b>73</b>	46 (23Tof)	<b>34</b> (17Tof)
Hamming <sub>15</sub> (med)	17	★	156 <sup>†</sup> (162 [16])	156	164 (82Tof)	<b>78</b> (35Tof + 8T)
HWB <sub>6</sub>	7	27	51 [16]	51	30 (15Tof)	<b>20</b> (10Tof)
Mod-Adder <sub>1024</sub>	28	★	798 <sup>†</sup> (978 [16])	<b>762</b>	570 (285Tof)	<b>500</b> (141Tof + 15CS + 188T)
Mod-Mult <sub>55</sub>	9	11	17 [16]	17*	14 (7Tof)	<b>6</b> (3Tof)
Mod-Red <sub>21</sub>	11	28	55 [16, 22]	<b>51</b>	34 (17Tof)	<b>22</b> (11Tof)
Mod 5 <sub>4</sub>	5	5	7 [19, 22, 23]	7*	8 (4Tof)	<b>2</b> (1Tof)
QCLA-Adder <sub>10</sub>	36	★	<b>116</b> [16]	135	<b>68</b> (34Tof)	94 (28Tof + 5CS + 28T)
QCLA-Com <sub>7</sub>	24	42	59 [16]	59	58 (29Tof)	<b>24</b> (12Tof)
QCLA-Mod <sub>7</sub>	26	★	<b>165</b> [16]	199	<b>118</b> (59Tof)	122 (43Tof + 36T)
QFT <sub>4</sub>	5	43	55 [16]	<b>53</b>	59 (2Tof + 55T)	<b>44</b> (4Tof + 3CS + 30T)
RC-Adder <sub>6</sub>	14	24	37 [16, 22]	37	22 (11Tof)	<b>12</b> (6Tof)
NC Toff <sub>3</sub>	5	7	13 [16, 22, 23]	13*	6 (3Tof)	<b>4</b> (2Tof)
NC Toff <sub>4</sub>	7	11	19 [16, 22, 23]	19*	10 (5Tof)	<b>6</b> (3Tof)
NC Toff <sub>5</sub>	9	15	25 [16]	25	14 (7Tof)	<b>8</b> (4Tof)
NC Toff <sub>10</sub>	19	35	55 [16]	55	34 (17Tof)	<b>18</b> (9Tof)
VBE-Adder <sub>3</sub>	10	14	20 [16, 22, 23]	<b>19</b> *	20 (10Tof)	<b>6</b> (3Tof)

**Table 2:** T-count achieved by different methods on a set of benchmark circuits. Even without gadgetization, AlphaTensor-Quantum matches or outperforms the considered baselines for all circuits that have not been split into sub-circuits (split circuits are marked with ★). When considering gadgets, AlphaTensor-Quantum further reduces the T-count drastically, and generally outperforms the original constructions with gadgets. The notation “ $a$ Tof+ $b$ CS+ $c$ T” indicates a circuit with  $a$  Toffoli gates,  $b$  CS gates, and  $c$  T gates (when multiple solutions from AlphaTensor-Quantum achieve the same T-count but differ in the trade-off between gadgets and T gates, we report the result with the highest number of Toffoli gates). Baseline results marked with † were obtained with the methods in Appendix B and are better than the best published T-count (provided in parentheses where applicable). Results marked with \* were proven to be optimal decompositions of the given tensor using the Z3 theorem prover.

### 3.2 Applications

We applied AlphaTensor-Quantum to circuits derived from several important use-cases for quantum computing, which fit into two broad categories: quantum implementations of classical reversible logic for arithmetic

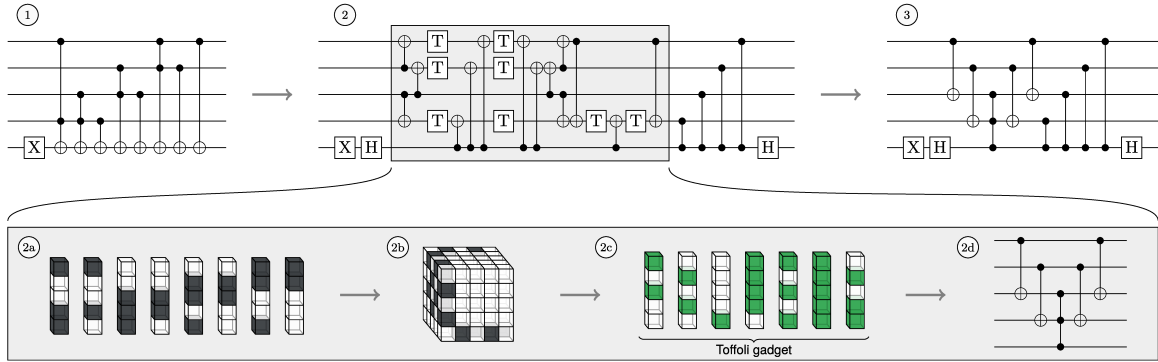


**Figure 3:** Results of AlphaTensor-Quantum on the Mod 54 circuit. **(1)** The original quantum circuit, which can be implemented with 4 Toffoli gates (with an equivalent cost of 8 T gates). **(2)** The compiled circuit, which has been split into Clifford gates and a subcircuit of just CNOT and T gates (in the highlighted box). **(2a)** The Waring decomposition corresponding to the highlighted CNOT+T circuit: each T gate corresponds precisely to one of the factors displayed as columns of blocks. **(2b)** The signature tensor formed from this decomposition. **(2c)** An alternative Waring decomposition of the tensor found by the RL agent. Again, each factor corresponds one-to-one to a T gate; however in this case the seven factors are grouped into a single Toffoli gadget. **(2d)** The quantum circuit obtained from this new decomposition. **(3)** The optimized circuit after having applied AlphaTensor-Quantum, which can be implemented using Clifford gates and a single Toffoli gate (i.e., its equivalent T-count is 2).

operations, and primitives important to quantum chemistry. We study the former because many quantum algorithms (for instance, Shor’s algorithm and many variations of Grover’s algorithm) require a quantum implementation of a classical oracle that performs some arithmetical or logical operation. We study the latter because quantum chemistry is a major application of quantum computing, and many of the state-of-the-art methods share similar circuit constructions.

**Multiplication in finite fields.** Multiplication in finite fields is a crucial operation for cryptography, since many elliptic-curve cryptography (ECC) implementations are built over such finite fields, and in fact these circuits are derived from a quantum algorithm that cracks ECC in polynomial time [27].

The results from Table 2 show that AlphaTensor-Quantum excels in optimizing the primitives for multiplication in finite fields of order  $2^m$ , i.e., the circuits  $\text{GF}(2^m)$ -mult. In Figure 4a, we show that for  $m = \{2, 3, 4, 5, 7\}$ , AlphaTensor-Quantum actually achieves the same Toffoli gate count as the best known *upper bound* for the equivalent classical (non-reversible) circuits [40, 41]. For  $m = \{2, 3, 4, 5\}$  this is also the best known *lower bound* [42], which suggests that the resulting quantum circuits are likely optimal. While the circuits for these targets were constructed using the naive  $\mathcal{O}(m^2)$  multiplication algorithm, the number of Toffoli gates of the optimized circuits follows  $\sim m^{\log_2(3)}$  for the considered values of  $m$ . Thus, AlphaTensor-Quantum found a multiplication algorithm with the same complexity as Karatsuba’s method [28], a *classical* algorithm for multiplication in finite fields. While it is conceivable to construct the resulting circuits by hand in principle, to the best of our knowledge no sub-quadratic constructions of quantum circuits for multiplication in finite fields have been discussed in the literature. AlphaTensor-Quantum finds them automatically, similar to Gidney’s

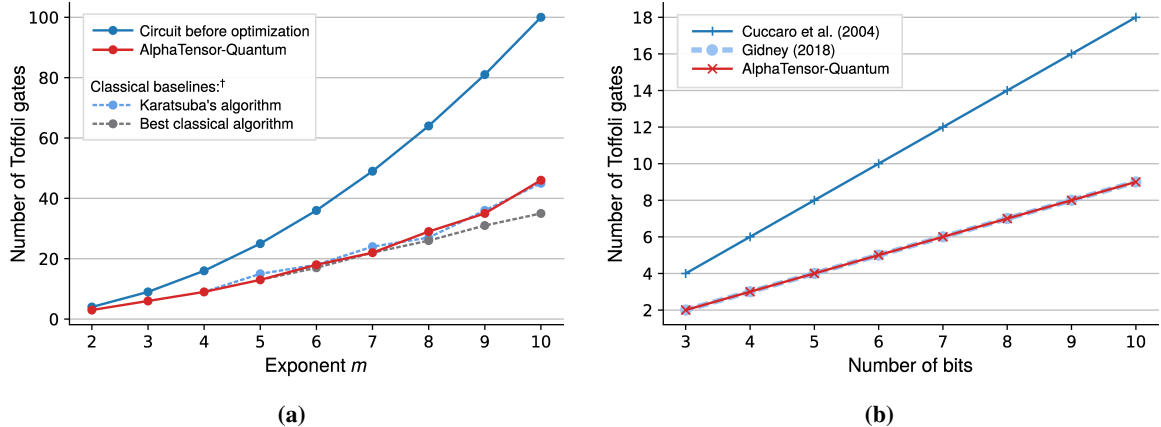


**Figure 4:** Number of Toffoli gates of the optimized circuits found by AlphaTensor-Quantum. **(a)** For multiplication in finite fields of order  $2^m$ , AlphaTensor-Quantum finds efficient circuits that significantly outperform the original construction, which scales like  $O(m^2)$ . The number of Toffoli gates matches the best known lower bound of the *classical* circuits [42] for some values of  $m$ , and scales as  $\sim m^{\log_2(3)}$ , showing that AlphaTensor-Quantum found an algorithm with the same complexity as Karatsuba’s method [28], a classical algorithm for multiplication on finite fields for which a quantum version has not been reported in the literature. (The baselines marked with † are classical circuits, and hence not directly comparable, as naive translations of classical to quantum circuits commonly introduce overheads. To compare, we assume the number of effective Toffoli gates is the number of 1-bit AND gates in the classical circuit.) **(b)** For binary addition, AlphaTensor-Quantum halves the cost of the circuits from Cuccaro et al. [43] matching the state-of-the-art circuits from Gidney [31]. Remarkably, it does so automatically without any prior knowledge of the measurement-based uncomputation technique, which was crucial to their results.

translation of Karatsuba’s method for multiplication of integers [30], but in contrast to the latter without requiring additionally ancilla qubits.

**Binary addition.** We apply AlphaTensor-Quantum to two different quantum implementations of the binary addition operation, which is a relevant primitive in oracle construction because many other common operations are built from it (such as multiplication, comparators, and modular arithmetic). For example, controlled addition circuits are the dominant cost of Shor’s algorithm. There are many types of quantum addition circuits (ripple-carry, carry-save, or block-carry-lookahead); we focus on ripple-carry addition circuits because they have fewer ancilla qubits generated by Hadamard gadgetization.

In particular, we optimize the circuits of Cuccaro et al. [43], which have a Toffoli count scaling as  $2n + O(1)$  where  $n$  is the number of input bits, as well as the circuits of Gidney [31], with a Toffoli count of  $n + O(1)$ . As shown in Figure 4b, AlphaTensor-Quantum reduces the Toffoli count of Cuccaro et al.’s circuits, matching the Toffoli count of Gidney’s construction of  $n + O(1)$ .

Prior to the publication of Gidney’s results, Cuccaro et al.’s circuits attained the lowest Toffoli count of any addition circuit. To halve their cost, Gidney introduced a new approach called *measurement-based uncomputation*, which allows Toffoli gates that were performed on zero-initialized ancilla qubits to be uncomputed for free under certain conditions, by introducing measurements and classically-controlled Clifford

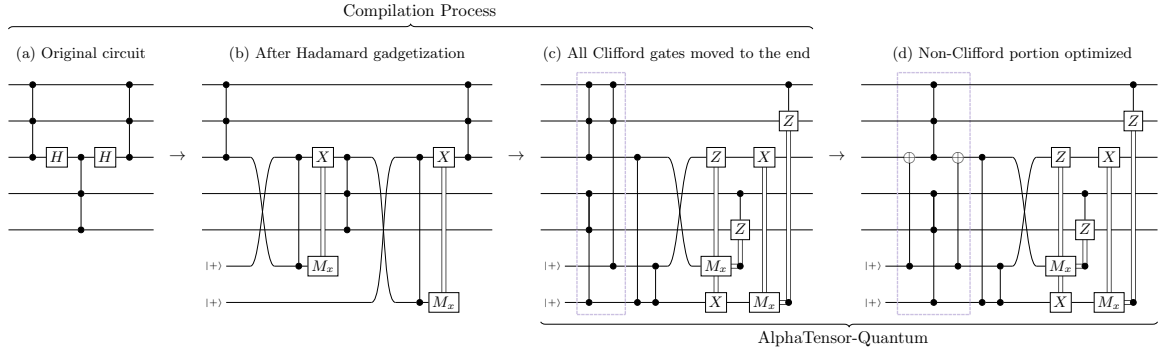


**Figure 5:** An example in which measurement-based uncomputation tricks can be recovered by AlphaTensor-Quantum. Here, a portion of the NC Toff<sub>3</sub> circuit is mapped to three CCZ gates, a pair of which share two inputs (in the highlighted box), by the Hadamard gadgetization process (detailed in Appendix C.1). AlphaTensor-Quantum optimizes this pair by expressing it as a single gadget, saving one Toffoli gate with respect to the original construction. This kind of optimization happens often because CCZ gates can usually be moved freely along the circuit, as the corresponding unitary matrix will be diagonal after compilation. This is reminiscent of the temporary logical-AND construction from Gidney [31], although some patterns with more than two CCZ gates can also be combined in this way.

gates. This non-trivial technique was invented more than a decade after the addition circuits of Cuccaro et al. [43], but is now widely used for optimizing fault-tolerant quantum circuits.

Importantly, for both circuit constructions, AlphaTensor-Quantum had no knowledge of measurement-based uncomputation, and all Toffoli gates were compiled naively using the standard unitary construction with seven T gates. Yet, AlphaTensor-Quantum automatically finds optimized circuits only accessible via measurement-based uncomputation. It does so with its ability to find Toffoli gadgets, by exploiting the fact that ancilla qubits from the Hadamard gadgetization allow the movement of Toffoli gates; see Figure 5 for an example.

**Hamming weight and phase gradients.** Applying small angle rotations to qubits is a common operation in quantum algorithms, e.g., in the quantum Fourier transform, data loading, and quantum chemistry. In fault-tolerant quantum circuits, any rotation can be implemented using the Solovay-Kitaev algorithm with a sequence of Hadamard and T gates. However, if the same small angle is to be applied repeatedly (such as in quantum chemistry), it is often more efficient to use a technique called Hamming weight phasing.

We use AlphaTensor-Quantum to optimize the Hamming weight phasing circuits from Gidney [31]. While the original circuits use measurement-based uncomputation, we instead compile a version where every Toffoli gate is constructed explicitly, as before. Again, AlphaTensor-Quantum halves the cost with respect to the naive input circuits, thus matching the complexity of the circuits with measurement-based uncomputation tricks.

**Unary iteration.** We also apply AlphaTensor-Quantum to a family of circuits called *unary iteration* [33]. These circuits allow selecting which Pauli operator (from a set of operators) to apply on the data qubits, based on the value of some control qubits. We apply this construction to the Pauli operators  $P_1 = XI \cdots I$ ,  $P_2 = IX \cdots I$ ,  $\dots$ ,  $P_m = II \cdots X$  on  $m = 8, 16$ , and  $32$  qubits, therefore implementing the quantum equivalent of a classical  $n$ -to- $2^n$  demultiplexer or decoder for  $n = 3, 4, 5$  (see Figure 6). These circuits could be used to

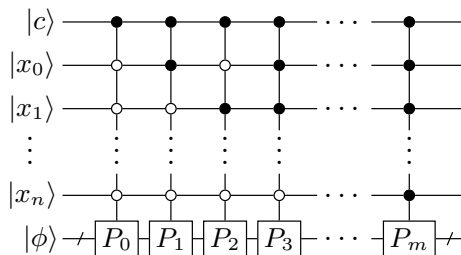


**Figure 6:** The action implemented by the unary iteration family of circuits. If the control qubit  $c$  is in the state  $|1\rangle$ , the circuit applies one of the Pauli operators from the set  $\{P_1, \dots, P_m\}$  to the multiqubit state  $|\phi\rangle$ , depending on the value of the qubits  $x_1$  to  $x_n$ . If the control qubit  $c$  is in the state  $|0\rangle$ , no operation is applied to  $|\phi\rangle$ .

implement the same construction for any set of 8, 16, or 32 Pauli operators, without extra T-count, and because of their generality, they appear both in oracle construction (demultiplexers are commonly used in classical logic) and in quantum chemistry (as in the linear combination of unitaries method discussed further below).

The unary iteration circuits were implemented following Babbush et al. [33], except we compiled the Toffoli gates unitarily with seven T gates instead of using measurement-based uncomputation. The largest circuit ( $n = 5$ ) has 72 qubits after compilation. As before, AlphaTensor-Quantum finds its own version of measurement-based uncomputation to match the best known T-count of these circuits.

We also apply a version of AlphaTensor-Quantum without gadgets. Remarkably, it finds optimized circuits that, for each value of  $n$ , have only three T gates more than the circuits from Babbush et al. [33] (where each Toffoli gate is implemented using four T gates), suggesting that the unary iteration circuits have an internal structure particularly amenable to this kind of optimization.

**Quantum chemistry.** Molecular simulation involves solving the Schrödinger equation, which requires a computational cost scaling exponentially with the number of particles in the system. This makes classical methods struggle to simulate strongly correlated molecules [44]. Quantum computers can theoretically handle these calculations more efficiently, with one compelling use case being the simulation of the FeMoco molecule, the active site in the nitrogenase enzyme responsible for nitrogen fixation. This use case has high potential industrial impact, but is challenging due to the highly complex electronic structure of FeMoco [45].

FeMoco simulation motivated Lee et al.’s [46] fault-tolerant implementation of a quantum walk-based algorithm. In this method, the Hamiltonian associated with the molecule is encoded into the quantum circuit with a technique known as *linear combination of unitaries* (LCU). This framework requires the implementation of two oracles called PREPARE and SELECT (each being an instance of the unary iteration operation discussed earlier). These are repeated many times, making up the dominant cost of the whole algorithm, and therefore optimizing these oracles can significantly impact the total resource requirements (see Appendix A for more details on the algorithm).

We run AlphaTensor-Quantum on portions of Lee et al.’s SELECT oracle construction (which is itself based on von Burg et al. [47]). Specifically, we set a range of parameters to keep the total qubit count below 60, and compile angle rotations of the state into the diagonal basis using the phase-gradient technique from Gidney [31]; see Figure 7 for details. As before, we remove all measurement-based uncomputation tricks and compile

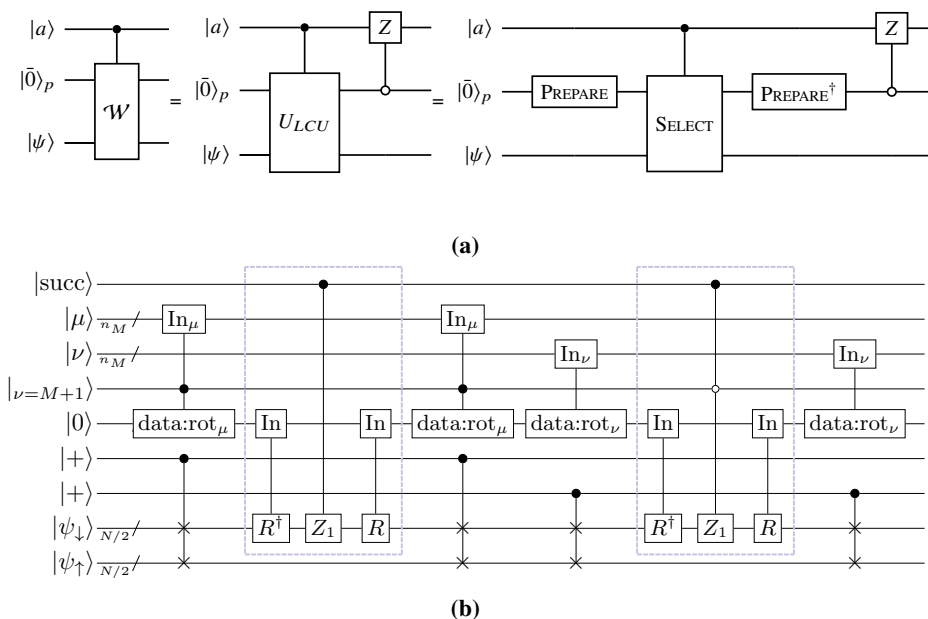


**Figure 7:** (a) The quantum walk operator  $\mathcal{W}$  at the heart of state-of-the-art quantum chemistry algorithms [33, 46, 48] (see Figure 9) can be decomposed using the LCU technique into two oracles,  $\text{PREPARE}$  and  $\text{SELECT}$ , which encode the details of the molecule. This operator is repeated many times, so its cost dominates the overall algorithm. (b) Construction of the  $\text{SELECT}$  oracle. This figure is adapted from Lee et al. [46, Figure 5, pp. 18]. We compile and optimize the part in the dashed box, along with its constituent components, for a range of parameters (up to 10 bits of precision per rotation, and for systems of up to 10 spin-orbitals).

the Toffoli gates unitarily with seven T gates. We find that, for all parameter values, AlphaTensor-Quantum is able to match the T-count of Lee et al. [46], which relies heavily on measurement-based uncomputation.

Thus, AlphaTensor-Quantum automatically finds state-of-the-art constructions for multiple use cases. We expect that, as new improvements on quantum chemistry are made at a structural level, AlphaTensor-Quantum will be able to automatically find the best constructions (in terms of T-count), without additional human effort.

## 4 Discussion

We have demonstrated the effectiveness of AlphaTensor-Quantum at optimizing the T-count, a key metric in quantum computations, showing that it significantly outperforms existing approaches, being able to automatically discover constructions as efficient as the best human-designed ones across various applications. For those applications, the fact that very different techniques achieve the same T-count might hint to the optimality of the discovered constructions. In fact, although AlphaTensor-Quantum does not come with optimality guarantees, we proved that some decompositions in Section 3.1 are optimal in terms of the number of factors of the decomposition.

Compared to previous works that use RL to optimize quantum circuits [49–51] or to improve variational quantum algorithms [52–56], Compared to previous works that use RL to optimize quantum circuits [49–51],

AlphaTensor-Quantum is the first one that scales to a large enough number of qubits to cover a wide range of applications (see Section 3.2), and the first one to consider fault-tolerant compilation. Compared to existing T-count optimization approaches, which are not RL-based, AlphaTensor-Quantum significantly outperforms them; however this comes at the cost of increased computational complexity (e.g., it took around 8 hours to optimize the addition circuits of Cuccaro et al. [43]) and loss of optimality due to extra compilation steps (e.g., if the circuits need to be split into parts). A possible future research avenue to accelerate the algorithm is to improve the neural network architecture; another avenue to scale up further is to handle Hadamard gadgetization differently, so that the number of qubits does not increase as much during the compilation process, or to apply RL to alternative circuit representations that can optimize Hadamard gates natively. However, we argue that its comparably increased computational complexity is outweighed by its results, especially considering the cost of manually designing optimized constructions. Moreover, it is a one-off cost: once AlphaTensor-Quantum has been applied, the optimized circuits can be reused.

Unlike existing approaches for T-count optimization, AlphaTensor-Quantum can leverage and exploit gadgets. These constructions are an active area of research [25, 26, 57, 58], and as fundamentally new gadgets are discovered, they can be readily incorporated into the RL environment, possibly allowing AlphaTensor-Quantum to discover even more efficient constructions for established quantum circuits. Similarly, due to its flexibility, AlphaTensor-Quantum can be extended to optimize metrics other than the T-count, such as T-depth [35] or weighted combinations of different types of gates [17], by changing the reward signal accordingly.

We envision AlphaTensor-Quantum will play a pivotal role as quantum chemistry and related fields advance, and new improvements at a structural level emerge. Similarly to how Gidney [31] optimized the addition circuits of Cuccaro et al. [43] over a decade later, AlphaTensor-Quantum finds and exploits non-trivial patterns, thus eliminating the need for manual construction design and saving research costs.

## 5 Methods

### 5.1 The Signature Tensor

The tensor representation of a circuit relies on the concept of *phase polynomials*. Consider a circuit with CNOT and T gates alone. Its corresponding unitary matrix  $U$  performs the operation  $U|x_{1:N}\rangle = e^{i\phi(x_{1:N})}Ax_{1:N}\rangle$ , where  $\phi(x_{1:N})$  is the phase polynomial and  $A$  is an invertible matrix that can be implemented with Clifford gates only. For example, applying a T gate to the second qubit after a CNOT gives  $(I \otimes T)CNOT|x, y\rangle = e^{i\frac{\pi}{4}(x \oplus y)}|x, x \oplus y\rangle$ , i.e.,  $\phi(x, y) = \frac{\pi}{4}(x \oplus y) = \frac{\pi}{4}(x + y - 2xy)$ . After cancelling out the terms leading to multiples of  $2\pi$ , the phase polynomial takes a multilinear form, i.e.,  $\phi(x_{1:N}) = \frac{\pi}{4} \left( \sum_i a_i x_i + 2 \sum_{i < j} b_{ij} x_i x_j + 4 \sum_{i < j < k} c_{ijk} x_i x_j x_k \right)$ , where  $a_i \in \{0, \dots, 7\}$ ,  $b_{ij} \in \{0, \dots, 3\}$ , and  $c_{ijk} \in \{0, 1\}$ . This maps directly to a circuit of T, CS and CCZ gates: each  $a_i x_i$  term is implemented by  $a_i$  T gates acting on the  $i$ -th qubit, each  $b_{ij} x_i x_j$  term corresponds to  $b_{ij}$  CS gates on qubits  $i$  and  $j$ , and each non-zero  $c_{ijk} x_i x_j x_k$  term is a CCZ gate on qubits  $i, j$ , and  $k$ . Each of these terms corresponds to a non-Clifford operation only if the corresponding constant ( $a_i$ ,  $b_{ij}$ , or  $c_{ijk}$ ) is odd. Thus, two CNOT + T circuits implement the same unitary up to Clifford gates if and only if they have the same phase polynomial after taking the modulo 2 of their coefficients. This information about the polynomial can then be captured in a symmetric 3-dimensional binary *signature tensor*  $\mathcal{T}$  of size  $N \times N \times N$  [16, 18]. See Appendix A for more details.

### 5.2 System Description

AlphaTensor-Quantum builds on AlphaTensor, which is in turn based on AlphaZero [59]. It is implemented over a distributed computing architecture, composed of one *learner* and multiple *actors* that communicate asynchronously. The learner is responsible for hosting a neural network and updating its parameters, while the main role of the actors is to play games in order to generate data for the learner. When the learner updates the network parameters by gradient descent steps, it sends them to the actors. The actors employ Monte Carlo tree search (MCTS), using queries to the network to guide their policy, and play games whose actions tend to improve over the policy dictated by the neural network. Played games are sent to the learner and stored in a buffer, and they will serve as future data points to train the network parameters.

**Neural network.** The neural network at the core of AlphaTensor-Quantum takes as input the game state and outputs: (i) a policy, i.e., a probability distribution over the next action to play, and (ii) a probability distribution over the estimated return (i.e., the sum of rewards from the current state until the end of the game); see Figure 8a. The neural network has a key component, the *torso*, where a set of attention operations [60] are applied. In AlphaTensor-Quantum, the torso interleaves two types of layers: axial attention [61] and *symmetrization layers* (Figure 8b). Symmetrization layers are inspired by the empirical observation that, for a symmetric input  $X \in \mathbb{R}^{N \times N}$  (with  $X = X^T$ ), preserving the symmetry of the output in-between axial attention layers significantly improves performance. Therefore, after each axial attention layer, we add a symmetrization operation, defined as  $X \leftarrow \beta \odot X + (1 - \beta) \odot X^T$ , where ‘ $\odot$ ’ denotes element-wise product. For  $\beta = \frac{1}{2}$ , this makes the output  $X$  symmetric. In practice, we found that letting  $\beta$  be a learnable  $N \times N$  matrix improves performance even further, even though  $X$  is no longer symmetric, due to the ability of the network to exchange information between rows and columns after each axial attention layer. (When the input is a tensor,  $X \in \mathbb{R}^{N \times N \times C}$ , we apply the symmetrization operations independently across the dimensions  $C$ , using

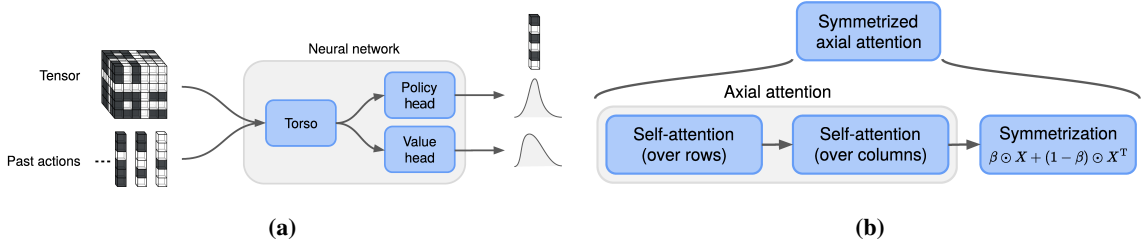


**Figure 8:** (a) An overview of the neural network, where the input is the current state (tensor and past actions) and the outputs are distributions over the next action to play (given by the policy head) and over the estimated return (given by the value head). (b) A symmetrized axial attention layer, the building block of the neural network torso. Symmetrized axial attention incorporates a symmetrization operation after each axial attention layer to favour exchange of information between rows and columns.

the same matrix  $\beta$ .) We refer to this architecture as *symmetrized axial attention*. See Appendix C.4 for more details of the full neural network architecture.

Symmetrized axial attention performs better than the neural network of standard AlphaTensor (which requires attention operations across every pair of modes of the tensor) [24]. It is also one of the key ingredients that allow AlphaTensor-Quantum to scale up to larger tensors: for  $N = 30$  and the same number of layers, symmetrized axial attention runs about 4x faster and reduces the memory consumption by a factor of 3x. (See also Appendix D.3 for further ablations.) We believe symmetrized axial attention may be useful for other applications beyond AlphaTensor-Quantum.

**Gadgetization patterns.** In TensorGame, every time an action is played, we check whether it completes a gadget to adjust the reward signal accordingly. If the action  $u^{(s)}$  at step  $s$  does not complete a gadget, the immediate reward is simply  $-1$ . Otherwise, the reward is  $+4$  if it completes a Toffoli, or  $0$  if it completes a CS gadget. These checks are done up to Clifford operations, and they involve finding certain linear dependencies between  $u^{(s)}$  and the previous actions:

- If  $s \geq 7$ , we check whether the action  $u^{(s)}$  completes a *Toffoli gadget*. Let  $a \triangleq u^{(s-6)}$ ,  $b \triangleq u^{(s-5)}$ , and  $c \triangleq u^{(s-4)}$ . If the vectors  $a$ ,  $b$ , and  $c$  are linearly independent and all the following relationships hold, then we declare that  $u^{(s)}$  completes a Toffoli gadget:

$$u^{(s-3)} = a + b, \quad u^{(s-2)} = a + c, \quad u^{(s-1)} = a + b + c, \quad \text{and} \quad u^{(s)} = b + c.$$

- If  $s \geq 3$ , we check whether the action  $u^{(s)}$  completes a *CS gadget*. Let  $a \triangleq u^{(s-2)}$  and  $b \triangleq u^{(s-1)}$ . If the vectors  $a$  and  $b$  are linearly independent and  $u^{(s)} = a + b$ , then  $u^{(s)}$  completes a CS gadget.

We refer to the relationships above as *gadgetization patterns* (see Appendix C.3 for a justification of these steps). Each factor (action) may belong to at most one gadget; thus, if the action at step  $s$  completes a gadget of any type, we only check for a new CS gadget from step  $s + 3$  onward, and for a new Toffoli gadget from step  $s + 7$  onward.

**Synthetic demonstrations.** Like its predecessor, AlphaTensor-Quantum uses a data set of randomly generated tensor/factorization pairs to train the neural network. Specifically, the network is trained on a mixture of a

supervised loss (which encourages it to imitate the synthetic demonstrations) and a standard RL loss (which encourages it to learn to decompose the target quantum signature tensor). For each experiment, we generate 5 million synthetic demonstrations. To generate each demonstration, we first randomly sample the number of factors  $R$  from a uniform distribution in  $[1, 125]$  and then sample  $R$  binary factors  $u^{(r)}$ , such that each element has a probability of 0.75 of being set to 0.

After having generated the factors, we randomly overwrite some of them to incorporate the patterns of the Toffoli and CS gadgets, in order to help the network learn and identify those patterns. For each demonstration, we include at least one gadget with probability 0.9. The number of gadgets is uniformly sampled in  $[1, 15]$  (the value is also truncated when  $R$  is not large enough), and for each gadget we sample the starting index  $r$  and the type of gadget (Toffoli with probability 0.6 and CS with probability 0.4), overwriting the necessary factors according to the gadget’s pattern. We ensure gadgets do not overlap throughout the demonstration.

**Change of basis.** To increase the diversity of the played games, the actors apply a random change of basis to the target tensor  $\mathcal{T}$  at the beginning of each game. From the quantum computation point of view, a change of basis can be implemented by a Clifford-only circuit, and therefore this procedure does not affect the resulting number of T gates.

A change of basis is represented by a matrix  $M \in \{0, 1\}^{N \times N}$  such that  $\det(M) = 1$  under modulo 2. We randomly generate 50 000 such basis changes and use them throughout the experiment, i.e., the actor first randomly picks a matrix  $M$  and then applies the following transformation to the target tensor  $\mathcal{T}$ :

$$\tilde{\mathcal{T}}_{ijk} = \sum_{a=1}^N \sum_{b=1}^N \sum_{c=1}^N M_{ia} M_{jb} M_{kc} \mathcal{T}_{abc}.$$

The actor then plays the game in that basis (i.e., it aims at finding a decomposition of  $\tilde{\mathcal{T}}$ ). After the game has finished, we can map the played actions back to the standard basis by applying the inverse change of basis.

The diversity injected by the change of basis facilitates the agent’s task, because it suffices to find a low-rank decomposition in any basis. Note that gadgets are not affected by the change of basis, since their patterns correspond to linear relationships that are preserved after linear transformations.

**Data augmentation.** For each game played by the actors, we obtain a new game by swapping two of the actions in it. Specifically, we swap the last action that is not part of a gadget with a randomly chosen action that is also not part of a gadget. Mathematically, swapping actions is a valid operation due to commutativity. From the quantum computation point of view, it is a valid operation because the considered unitary matrices are diagonal.

Besides the action permutation, we also permute the inputs at acting time every time we query the neural network. In particular, we apply a random permutation to the input tensor and past actions that represent the current state, and then invert this permutation at the output of the network’s policy head. Similarly, at training time, we apply a random permutation to both the input and the policy targets, and train the neural network on this transformed version of the data. In practice, we sample 100 permutations at the beginning of an experiment, and use them thereafter.

**Sample-based MCTS.** In AlphaTensor-Quantum, the action space is huge, and therefore it is not possible to enumerate all the possible actions from a given state. Instead, AlphaTensor-Quantum relies on sample-based MCTS, similarly to sampled AlphaZero [62].

Before committing to an action, the agent uses a *search tree* to explore multiple actions to play. Each node in the tree represents a state, and each edge represents an action. For each state-action pair  $(s, a)$ , we store a set of statistics: the visit count  $N(s, a)$ , the action value  $Q(s, a)$ , and the empirical policy probability  $\hat{\pi}(s, a)$ . The search consists of multiple simulations; each simulation traverses the tree from the root state  $s_0$  until a leaf state  $s_L$  is reached, by recursively selecting in each state  $s$  an action  $a$  that has high empirical policy probability and high value but has not been frequently explored, i.e., we choose  $a$  according to

$$\arg \max_a Q(s, a) + c(s) \hat{\pi}(s, a) \frac{\sqrt{\sum_b N(s, b)}}{1 + N(s, a)},$$

where  $c(s)$  is an exploration factor. The MCTS simulation keeps choosing actions until a leaf state  $s_L$  is reached; when that happens, the network is queried on  $s_L$  — obtaining the policy probability  $\pi(s_L, \cdot)$  and the return probability  $z(s_L)$ . We sample  $K$  actions  $a_k$  from the policy to initialize  $\hat{\pi}(s_L, a) = \frac{1}{K} \sum_k \delta_{a, a_k}$ , and initialize  $Q(s_L, a)$  from  $z(s_L)$  using a risk-seeking value [24]. After the node  $s_L$  has been expanded, we update the visit counts and values on the simulated trajectory in a backward pass [62]. We simulate 800 trajectories using MCTS; after that, we use the visit counts of the actions at the root of the search tree to form a sample-based improved policy, following Fawzi et al. [24], and commit to an action sampled from that improved policy.

**Training regime.** We train AlphaTensor-Quantum on a TPU with 256 cores, with a total batch size of 2 048, training for 1 million iterations on average (the number of training iterations varies depending on the application, ranging between 80 000 and 3 million iterations). We use 3 600 actors on average per experiment, each running on a standalone TPU. Each experiment is ran on a set of target tensors, which we group by application (i.e., one experiment for addition, one for unary iteration, etc.); this allows the RL agent to recognize and exploit the decomposition patterns that might be present across multiple tensors within the same experiment. We find that the experiment variance is very low: a single experiment is enough for AlphaTensor-Quantum to find the best constructions for each application.

**Other versions of AlphaTensor-Quantum.** We found empirically that the  $\text{GF}(2^m)$ -mult circuits were particularly challenging to optimize, and they required additional training iterations. To reduce the size of the search space and accelerate the training procedure, we developed a variant of AlphaTensor-Quantum that significantly favours Toffoli gates. Specifically, every time that three consecutive and linearly independent actions (factors) are played, the environment automatically applies the remaining four actions that would complete the Toffoli gadget. We applied this version of AlphaTensor-Quantum to optimize these targets only.

### 5.3 Verification

In order to verify that the results of AlphaTensor-Quantum are correct, we used the `feynver` tool developed by Amy [36] after each step of the compilation process discussed in Appendix C.1. It uses the sum-over-paths formalism [63] to produce a proof of equality and can be applied to any circuit. However, it is a sound but not

complete method, so it may fail both to prove and to disprove equality for some pairs of circuits. Since the tool runs slowly for larger circuits, we ran it wherever practical (limiting each run to several hours). Each circuit was verified assuming that any intermediate measurements introduced by Hadamard gadgetization always return zero, because our software pipeline does not generate the classically-controlled correction circuits (these can be easily constructed but are irrelevant to AlphaTensor-Quantum).

This allowed us to verify inputs up to the point where a tensor is obtained. In order to verify that the decompositions constructed by AlphaTensor-Quantum were correct, we computed the corresponding tensor and checked that it was equal to the original input tensor. While we did not use the optimized decompositions to produce circuits, they could be verified in the same way as discussed above.

## Acknowledgements

The authors thank Steve Clark, Alexander L. Gaunt, Alexandre Krajenbrink, Luca Mondada, and Richie Yeung for their feedback on the paper; and Ryan Babbush, Sergio Boixo, Craig Gidney, Matt Harrigan, Tanuj Khattar, and Nicholas Rubin for insightful discussions and ideas.

## References

- [1] Richard P Feynman. Simulating physics with computers. *International journal of theoretical physics*, 21(6/7):467–488, 1982.
- [2] Yuri Manin. *Computable and noncomputable*. Sovetskoe Radio, 1980.
- [3] Peter W. Shor. Polynomial-time algorithms for prime factorization and discrete logarithms on a quantum computer. *SIAM Journal on Computing*, 26(5):1484–1509, October 1997. ISSN 1095-7111. doi: 10.1137/s0097539795293172.
- [4] Nick S. Blunt, Joan Camps, Ophelia Crawford, Róbert Izsák, Sebastian Leontica, Arjun Mirani, Alexandra E. Moylett, Sam A. Scivier, Christoph Sünderhauf, Patrick Schopf, Jacob M. Taylor, and Nicole Holzmann. Perspective on the current state-of-the-art of quantum computing for drug discovery applications. *Journal of Chemical Theory and Computation*, 18(12):7001–7023, November 2022. ISSN 1549-9626. doi: 10.1021/acs.jctc.2c00574.
- [5] Alexander M. Dalzell, Sam McArdle, Mario Berta, Przemyslaw Bienias, Chi-Fang Chen, András Gilyén, Connor T. Hann, Michael J. Kastoryano, Emil T. Khabiboulline, Aleksander Kubica, Grant Salton, Samson Wang, and Fernando G. S. L. Brandão. Quantum algorithms: A survey of applications and end-to-end complexities, 2023.
- [6] Sergey Bravyi and Alexei Kitaev. Universal quantum computation with ideal Clifford gates and noisy ancillas. *Physical Review A*, 71:022316, 2005.
- [7] Earl T. Campbell, Barbara M. Terhal, and Christophe Vuillot. Roads towards fault-tolerant universal quantum computation. *Nature*, 549(7671):172–179, September 2017. ISSN 1476-4687. doi: 10.1038/nature23460.

- [8] Craig Gidney and Austin G. Fowler. Efficient magic state factories with a catalyzed  $|CCZ\rangle$  to  $2|T\rangle$  transformation. *Quantum*, 3:135, 2019.
- [9] Daniel Gottesman. The Heisenberg representation of quantum computers. *arXiv preprint arXiv:quant-ph/9807006*, 1998.
- [10] A. R. Calderbank and Peter W. Shor. Good quantum error-correcting codes exist. *Physical Review A*, 54(2):1098–1105, August 1996. ISSN 1094-1622. doi: 10.1103/physreva.54.1098.
- [11] Dorit Aharonov and Michael Ben-Or. Fault tolerant quantum computation with constant error, 1996.
- [12] Bryan Eastin and Emanuel Knill. Restrictions on transversal encoded quantum gate sets. *Physical Review Letters*, 102(11), March 2009. ISSN 1079-7114. doi: 10.1103/physrevlett.102.110502.
- [13] John van de Wetering and Matthew Amy. Optimising T-count is NP-hard. *arXiv preprint arXiv:2310.05958*, 2023.
- [14] Matthew Amy, Dmitri Maslov, and Michele Mosca. Polynomial-time T-depth optimization of clifford+T circuits via matroid partitioning. *arXiv preprint arXiv:1303.2042*, 2013.
- [15] David Gosset, Vadym Kliuchnikov, Michele Mosca, and Vincent Russo. An algorithm for the T-count. *Quantum Information & Computation*, 14(15–16):1261–1276, nov 2014.
- [16] Luke E. Heyfron and Earl T. Campbell. An efficient quantum compiler that reduces T count. *Quantum Science and Technology*, 4(1):015004, sep 2018.
- [17] Yunseong Nam, Neil J. Ross, Yuan Su, Andrew M. Childs, and Dmitri Maslov. Automated optimization of large quantum circuits with continuous parameters. *npj Quantum Information*, 4(23), 2018.
- [18] Matthew Amy and Michele Mosca. T-count optimization and Reed-Muller codes. *IEEE Transactions on Information Theory*, 65(8):4771–4784, 2019.
- [19] Aleks Kissinger and John van de Wetering. Reducing T-count with the ZX-calculus. *arXiv preprint arXiv:1903.10477*, 2019.
- [20] Vlad Gheorghiu, Michele Mosca, and Priyanka Mukhopadhyay. T-count and T-depth of any multi-qubit unitary. *npj Quantum Information*, 8(141), 2022.
- [21] Aleks Kissinger and John van de Wetering. Simulating quantum circuits with ZX-calculus reduced stabiliser decompositions. *Quantum Science and Technology*, 7:044001, 2022.
- [22] Neil de Beaudrap, Xiaoning Bian, and Quanlong Wang. Techniques to reduce  $\pi/4$ -parity-phase circuits, motivated by the ZX calculus. *arXiv preprint arXiv:1911.09039*, 2019.
- [23] Niel de Beaudrap, Xiaoning Bian, and Quanlong Wang. Fast and effective techniques for T-count reduction via spider nest identities. In *Conference on the Theory of Quantum Computation, Communication and Cryptography*, volume 158, pages 11:1–11:23, 2020.

- [24] Alhussein Fawzi, Matej Balog, Aja Huang, Thomas Hubert, Bernardino Romera-Paredes, Mohammadamin Barekatalin, Alexander Novikov, Francisco J. R. Ruiz, Julian Schrittwieser, Grzegorz Swirszcz, David Silver, Demis Hassabis, and Pushmeet Kohli. Discovering faster matrix multiplication algorithms with reinforcement learning. *Nature*, 610:47–53, 2022.
- [25] Cody Jones. Low-overhead constructions for the fault-tolerant Toffoli gate. *Physical Review A*, 87(2), 2013.
- [26] Michael Beverland, Earl Campbell, Mark Howard, and Vadym Kliuchnikov. Lower bounds on the non-Clifford resources for quantum computations. *Quantum Science and Technology*, 5(3), 2020.
- [27] Donny Cheung, Dmitri Maslov, Jimson Mathew, and Dhiraj K. Pradhan. On the design and optimization of a quantum polynomial-time attack on elliptic curve cryptography. In *Theory of Quantum Computation, Communication, and Cryptography*, volume 5106, pages 96–104, 2008.
- [28] Anatoly Karatsuba and Yuri Ofman. Multiplication of many-digital numbers by automatic computers. *Proceedings of the USSR Academy of Sciences*, 145:293–294, 1962.
- [29] Charles H Bennett. Time/space trade-offs for reversible computation. *SIAM J. Comput.*, 18(4):766–776, August 1989.
- [30] Craig Gidney. Asymptotically efficient quantum Karatsuba multiplication, 2019.
- [31] Craig Gidney. Halving the cost of quantum addition. *Quantum*, 2(74), 2018.
- [32] Markus Reiher, Nathan Wiebe, Krysta M. Svore, Dave Wecker, and Matthias Troyer. Elucidating reaction mechanisms on quantum computers. *Proceedings of the National Academy of Sciences*, 114(29): 7555–7560, 2017.
- [33] Ryan Babbush, Craig Gidney, Dominic W. Berry, Nathan Wiebe, Jarrod McClean, Alexandru Paler, Austin Fowler, and Hartmut Neven. Encoding electronic spectra in quantum circuits with linear t complexity. *Physical Review X*, 8:041015, Oct 2018.
- [34] Vivien Vandaele, Simon Martiel, Simon Perdrix, and Christophe Vuillot. Optimal Hadamard gate count for Clifford+T synthesis of Pauli rotations sequences. *arXiv preprint arXiv:2302.07040*, 2023.
- [35] Matthew Amy, Dmitri Maslov, Michele Mosca, and Martin Roetteler. A meet-in-the-middle algorithm for fast synthesis of depth-optimal quantum circuits. *IEEE Transactions on Computer-Aided Design of Integrated Circuits and Systems*, 32(6):818–830, 2013.
- [36] Matthew Amy. Feynman. <https://github.com/meamy/feynman>, 2016.
- [37] Fang Zhang and Jianxin Chen. Optimizing T gates in Clifford+T circuit as  $\pi/4$  rotations around Paulis. *arXiv preprint arXiv:quant-ph/1903.12456*, 2019.
- [38] Anthony Munson, Bob Coecke, and Quanlong Wang. AND-gates in ZX-calculus: Spider nest identities and QBC-completeness. In *Quantum Physics and Logic*, 2020.

- [39] Leonardo de Moura and Nikolaj Bjørner. Z3: An efficient SMT solver. In C. R. Ramakrishnan and Jakob Rehof, editors, *Tools and Algorithms for the Construction and Analysis of Systems*, pages 337–340, Berlin, Heidelberg, 2008. Springer Berlin Heidelberg. ISBN 978-3-540-78800-3.
- [40] Peter L. Montgomery. Five, six, and seven-term Karatsuba-like formulae. *IEEE Transactions on Computers*, 54(3):362–369, 2005.
- [41] Haining Fan and M. Anwar Hasan. Comments on “five, six, and seven-term Karatsuba-like formulae”. *IEEE Transactions on Computers*, 56(5):716–717, 2007. doi: 10.1109/TC.2007.1024.
- [42] Razvan Barbulescu, Jérémie Detrey, Nicolas Estibals, and Paul Zimmermann. Finding optimal formulae for bilinear maps. In Ferruh Özbudak and Francisco Rodríguez-Henríquez, editors, *Arithmetic of Finite Fields*, pages 168–186, Berlin, Heidelberg, 2012. Springer Berlin Heidelberg. ISBN 978-3-642-31662-3.
- [43] Steven A. Cuccaro, Thomas G. Draper, Samuel A. Kutin, and David Petrie Moulton. A new quantum ripple-carry addition circuit. *arXiv preprint arXiv:quant-ph/0410184*, 2004.
- [44] Román Orús. Tensor networks for complex quantum systems. *Nature Reviews Physics*, 1(9):538–550, 2019. doi: 10.1038/s42254-019-0086-7.
- [45] Markus Reiher, Nathan Wiebe, Krysta M. Svore, Dave Wecker, and Matthias Troyer. Elucidating reaction mechanisms on quantum computers. *Proceedings of the National Academy of Sciences*, 114(29):7555–7560, 2017. doi: 10.1073/pnas.1619152114.
- [46] Joonho Lee, Dominic W. Berry, Craig Gidney, William J. Huggins, Jarrod R. McClean, Nathan Wiebe, and Ryan Babbush. Even more efficient quantum computations of chemistry through tensor hypercontraction. *PRX Quantum*, 2:030305, Jul 2021. doi: 10.1103/PRXQuantum.2.030305.
- [47] Vera von Burg, Guang Hao Low, Thomas Häner, Damian S. Steiger, Markus Reiher, Martin Roetteler, and Matthias Troyer. Quantum computing enhanced computational catalysis. *Phys. Rev. Res.*, 3:033055, Jul 2021. doi: 10.1103/PhysRevResearch.3.033055.
- [48] Dominic W. Berry, Craig Gidney, Mario Motta, Jarrod R. McClean, and Ryan Babbush. Qubitization of Arbitrary Basis Quantum Chemistry Leveraging Sparsity and Low Rank Factorization. *Quantum*, 3:208, December 2019. ISSN 2521-327X. doi: 10.22331/q-2019-12-02-208.
- [49] Lorenzo Moro, Matteo G. A. Paris, Marcello Restelli, and Enrico Prati. Quantum compiling by deep reinforcement learning. *Communications Physics*, 4(1):178, 2021. doi: 10.1038/s42005-021-00684-3.
- [50] Thomas Fösel, Murphy Y. Niu, Floriand Marquardt, and Li Li. Quantum circuit optimization with deep reinforcement learning. *arXiv preprint arXiv:quant-ph/2103.07585*, 2021.
- [51] Nils Quetschlich, Lukas Burgholzer, and Robert Wille. Compiler optimization for quantum computing using reinforcement learning, 2023.
- [52] Mateusz Ostaszewski, Lea M. Trenkwalder, Wojciech Masarczyk, Eleanor Scerri, and Vedran Dunjko. Reinforcement learning for optimization of variational quantum circuit architectures. In M. Ranzato, A. Beygelzimer, Y. Dauphin, P.S. Liang, and J. Wortman Vaughan, editors, *Advances in Neural Information Processing Systems*, volume 34, pages 18182–18194. Curran Associates, Inc., 2021.

- [53] En-Jui Kuo, Yao-Lung L. Fang, and Samuel Y.-C. Chen. Quantum architecture search via deep reinforcement learning. *arXiv preprint arXiv:quant-ph/2104.07715*, 2021.
- [54] Xianchao Zhu and Xiaokai Hou. Quantum architecture search via truly proximal policy optimization. *Scientific Reports*, 13(1):5157, 2023. doi: 10.1038/s41598-023-32349-2.
- [55] Jiahao Yao, Haoya Li, Marin Bukov, Lin Lin, and Lexing Ying. Monte Carlo tree search based hybrid optimization of variational quantum circuits. In Bin Dong, Qianxiao Li, Lei Wang, and Zhi-Qin John Xu, editors, *Proceedings of Mathematical and Scientific Machine Learning*, volume 190 of *Proceedings of Machine Learning Research*, pages 49–64. PMLR, 15–17 Aug 2022.
- [56] Bodo Rosenhahn and Tobias J. Osborne. Monte Carlo graph search for quantum circuit optimization. *Phys. Rev. A*, 108:062615, Dec 2023. doi: 10.1103/PhysRevA.108.062615.
- [57] Craig Gidney and Cody Jones. A CCCZ gate performed with 6 T gates. *arXiv preprint arXiv:2106.11513*, 2021.
- [58] Matthew Amy and Neil J. Ross. Phase-state duality in reversible circuit design. *Physical Review A*, 104:052602, Nov 2021.
- [59] David Silver, Thomas Hubert, Julian Schrittwieser, Ioannis Antonoglou, Matthew Lai, Arthur Guez, Marc Lanctot, Laurent Sifre, Dhharshan Kumaran, Thore Graepel, Timothy Lillicrap, Karen Simonyan, and Demis Hassabis. A general reinforcement learning algorithm that masters chess, shogi, and Go through self-play. *Science*, 362(6419):1140–1144, 2018.
- [60] Ashish Vaswani, Noam Shazeer, Niki Parmar, Jakob Uszkoreit, Llion Jones, Aidan N Gomez, Lukasz Kaiser, and Illia Polosukhin. Attention is all you need. In *Advances in Neural Information Processing Systems*, 2017.
- [61] Jonathan Ho, Nal Kalchbrenner, Dirk Weissenborn, and Tim Salimans. Axial attention in multidimensional transformers. *arXiv preprint arXiv:1912.12180*, 2019.
- [62] Thomas Hubert, Julian Schrittwieser, Ioannis Antonoglou, Mohammadamin Barekatain, Simon Schmitt, and David Silver. Learning and planning in complex action spaces. In *International Conference on Machine Learning*, pages 4476–4486, 2021.
- [63] Christopher M. Dawson, Andrew P. Hines, Duncan Mortimer, Henry L. Haselgrove, Michael A. Nielsen, and Tobias J. Osborne. Quantum computing and polynomial equations over the finite field  $\mathbb{Z}_2$ . *Quantum Info. Comput.*, 5(2):102–112, mar 2005. ISSN 1533-7146.
- [64] Yuan Su, Dominic W. Berry, Nathan Wiebe, Nicholas Rubin, and Ryan Babbush. Fault-tolerant quantum simulations of chemistry in first quantization. *PRX Quantum*, 2:040332, Nov 2021. doi: 10.1103/PRXQuantum.2.040332.
- [65] Mark Steudtner, Sam Morley-Short, William Pol, Sukin Sim, Cristian L. Cortes, Matthias Loipersberger, Robert M. Parrish, Matthias Degroote, Nikolaj Moll, Raffaele Santagati, and Michael Streif. Fault-tolerant quantum computation of molecular observables. *Quantum*, 7:1164, November 2023. ISSN 2521-327X. doi: 10.22331/q-2023-11-06-1164.

- [66] Ronald de Wolf. Quantum computing: Lecture notes, 2019.
- [67] Bela Bauer, Sergey Bravyi, Mario Motta, and Garnet Kin-Lic Chan. Quantum algorithms for quantum chemistry and quantum materials science. *Chemical Reviews*, 120(22):12685–12717, October 2020. ISSN 1520-6890. doi: 10.1021/acs.chemrev.9b00829. URL <http://dx.doi.org/10.1021/acs.chemrev.9b00829>.
- [68] Seunghoon Lee, Joonho Lee, Huanchen Zhai, Yu Tong, Alexander M. Dalzell, Ashutosh Kumar, Phillip Helms, Johnnie Gray, Zhi-Hao Cui, Wenyuan Liu, Michael Kastoryano, Ryan Babbush, John Preskill, David R. Reichman, Earl T. Campbell, Edward F. Valeev, Lin Lin, and Garnet Kin-Lic Chan. Evaluating the evidence for exponential quantum advantage in ground-state quantum chemistry. *Nature Communications*, 14(1):1952, 2023. doi: 10.1038/s41467-023-37587-6.
- [69] Andrew M. Childs and Nathan Wiebe. Hamiltonian simulation using linear combinations of unitary operations. *Quantum Info. Comput.*, 12(11–12):901–924, nov 2012. ISSN 1533-7146.
- [70] Guang Hao Low, Vadym Kliuchnikov, and Luke Schaeffer. Trading T-gates for dirty qubits in state preparation and unitary synthesis. *arXiv preprint arXiv:1812.00954*, 2018.
- [71] Guang Hao Low and Isaac L. Chuang. Hamiltonian Simulation by Qubitization. *Quantum*, 3:163, July 2019. ISSN 2521-327X. doi: 10.22331/q-2019-07-12-163. URL <https://doi.org/10.22331/q-2019-07-12-163>.
- [72] John van de Wetering, Richie Yeung, Tuomas Laakkonen, and Aleks Kissinger. Optimal compilation of parametrised quantum circuits. *arXiv preprint arXiv:2401.12877*, 2024.
- [73] Vivien Vandaele, Simon Martiel, and Timothée Goubault de Brugière. Phase polynomials synthesis algorithms for NISQ architectures and beyond. *Quantum Science and Technology*, 7(4):045027, sep 2022.
- [74] Arianne Meijer-van de Griend and Ross Duncan. Architecture-aware synthesis of phase polynomials for NISQ devices. *arXiv preprint arXiv:quant-ph/2004.06052*, 2020.
- [75] Giulia Meuli, Mathias Soeken, and Giovanni De Micheli. Sat-based {cnot, t} quantum circuit synthesis. In Jarkko Kari and Irek Ulidowski, editors, *Reversible Computation*, pages 175–188, Cham, 2018. Springer International Publishing.

## A Additional Background

### A.1 Quantum Computing

**Qubits.** While a classical computer works on bits 0 and 1, a quantum computer works with qubits, which are superpositions of 0 and 1, representable by a normalized vector in the vector space  $\mathbb{C}^2$ . We write  $|0\rangle, |1\rangle \in \mathbb{C}^2$  for the standard basis vectors. Generally, we adopt *bra-ket* notation, and write  $|\psi\rangle = a|0\rangle + b|1\rangle$  (with  $a, b \in \mathbb{C}$ ) for any normalized complex vector (i.e., with  $|a|^2 + |b|^2 = 1$ ). When we have two qubits, its state space is given by tensor product of the spaces for a single qubit:  $\mathbb{C}^2 \otimes \mathbb{C}^2 \cong \mathbb{C}^{2^2}$ . Generally, the  $N$ -qubit state space consists of the normalized vectors in  $\mathbb{C}^{2^N}$ . A basis for this space is given by the states  $|\vec{x}\rangle$  given by bit strings  $\vec{x} \in \{0, 1\}^N$ .

**Quantum gates.** State transformations in quantum computing are linear operations that preserve the normalization, and hence map quantum states to quantum states. These operations are fully represented by unitary matrices. Besides the common examples from the main paper, such as the Hadamard gate or the X gate, we define the  $Z[\alpha]$  phase gate as

$$Z[\alpha] = \begin{pmatrix} 1 & 0 \\ 0 & e^{i\alpha} \end{pmatrix}.$$

We use the notation  $Z[\alpha]$  to explicitly indicate that the gate is parameterized by  $\alpha \in \mathbb{R}$ , so that  $Z[\alpha]|\psi\rangle = aZ[\alpha]|0\rangle + bZ[\alpha]|1\rangle = a|0\rangle + be^{i\alpha}|1\rangle$ . In contrast, when we refer to the (unparameterized) Z gate, we assume the special case  $\alpha = \pi$ , i.e.,  $Z \equiv Z[\pi]$ , such that  $Z|\psi\rangle = a|0\rangle - b|1\rangle$ . The T gate and the S gate are also phase gates, with  $\alpha = \pi/4$  and  $\alpha = \pi/2$ , respectively.

**Controlled gates.** As explained in the main paper, the controlled gates are two-qubit gates that only perform a non-trivial action on the second qubit if the first qubit is in the  $|1\rangle$  state. For instance, the CNOT gate performs a NOT gate on the second qubit if the first qubit is  $|1\rangle$ . We can write this succinctly as  $CNOT|x, y\rangle = |x, x \oplus y\rangle$ . Similarly, the CZ gate implements a Z phase gate on the second qubit if the first is in the  $|1\rangle$  state, i.e.,  $CZ|x, y\rangle = (-1)^{xy}|x, y\rangle$ , where here we write a juxtaposition of bits  $xy$  to denote their AND. More generally, the controlled  $Z[\alpha]$  phase gate acts as  $CZ[\alpha]|x, y\rangle = e^{i\alpha xy}|x, y\rangle$ . We also consider the controlled CNOT gate, also called Toffoli gate, whose action is  $Tof|x, y, z\rangle = |x, y, (xy) \oplus z\rangle$ . Similarly, the controlled CZ gate acts as  $CCZ|x, y, z\rangle = (-1)^{xyz}|x, y, z\rangle$ .

**Universal gate sets.** The Hadamard  $H$ , CNOT, and the Z phase gates  $Z[\alpha]$  form a *universal* gate set, meaning that any unitary matrix, and hence any quantum computation, can be decomposed into these gates. For instance, we have  $X = HZ[\pi]H$ .

In fault-tolerant quantum computation we cannot use a continuous family of gates like  $Z[\alpha]$ , and instead work with a small discretized set of quantum gates. A particularly often used one is the T gate,  $T \triangleq Z[\frac{\pi}{4}]$ . The gate set consisting of  $H$ , CNOT and  $T$  is an *approximately universal* gate set, meaning that any unitary can be approximated arbitrarily well by a circuit consisting of these gates.

**Clifford + T.** While quantum computing is generally believed to be hard to classically simulate, there is a useful subset of quantum computations for which there is an efficient classical simulation algorithm. These are known as *Clifford* computations, and they are built out of Clifford gates. The Clifford gates are H, CNOT, and

S. For this reason, an often-used approximately universal gate set is  $\{H, \text{CNOT}, S, T\}$ , which is called the Clifford+T gate set. As the Clifford gates are efficiently simulable, the number of T gates is a measure of how hard it is to perform the computation classically.

More concretely, T gates are also the hardest gates to execute: in most fault-tolerant architectures for quantum computation, the Clifford gates are relatively easy to perform, while T gates cost orders-of-magnitude more resources. This is because Clifford gates can be executed “natively” in many error-correcting codes, while T gates are implemented by injecting a magic state that first has to be distilled to a desired precision.

**T gate optimization.** For this reason it is important to reduce the number of T gates required for a computation as much as possible. There are several ways to do this. For instance, since  $S = T^2$ , whenever two T gates appear in a row, they combine to form a Clifford gate. More generally, if we have  $T^k$ , then this costs just one T gate if  $k$  is odd, and is Clifford otherwise. This technique for combining T gates can be generalized to settings where they do not appear directly after one another on the same qubit—which is a restrictive consideration. The generalization can be used to combine T gates that are applied to the same *parity*.

Recall the actions of the  $Z[\alpha]$  and CNOT gates. Considering  $x, y \in \{0, 1\}$ , we have  $Z[\alpha]|x\rangle = e^{i\alpha x}|x\rangle$  and  $\text{CNOT}|x, y\rangle = |x, x \oplus y\rangle$ . Thus, if we apply a  $Z[\alpha]$  gate to the second qubit after a CNOT, it applies a phase to the parity  $x \oplus y$ , i.e.,  $(I \otimes Z[\alpha])\text{CNOT}|x, y\rangle = (I \otimes Z[\alpha])|x, x \oplus y\rangle = e^{i\alpha(x \oplus y)}|x, x \oplus y\rangle$ .

More generally, when we have a circuit consisting of just CNOT and  $Z[\alpha]$  phase gates, the unitary matrix  $U$  that it implements acts as  $U|\vec{x}\rangle = e^{i\phi(\vec{x})}|A\vec{x}\rangle$ , where  $\phi : \{0, 1\}^n \rightarrow \mathbb{R}$  is a *phase polynomial*, and  $A$  is an invertible matrix that can be implemented with Clifford operations. Using this phase polynomial representation, phase gates that are implicitly acting on the same parity get combined. When we then resynthesize a quantum circuit from this representation, we hence possibly require fewer phase gates.

**Multilinear phase polynomials.** When we construct a phase polynomial from a CNOT +  $Z[\alpha]$  circuit in this way, we get a phase polynomial consisting of XOR terms. This representation is not unique. As a simple example, we can see that  $e^{i\pi(x+y+x\oplus y)} = e^{2\pi i} = 1$  for all  $x, y \in \{0, 1\}$ . If we were to directly synthesize the first expression, this would require three phase gates corresponding to the three terms ( $x$ ,  $y$ , and  $x \oplus y$ ), even though it implements an identity. We can rewrite the phase polynomial into a unique form by decomposing each of the XOR terms into a *multilinear* form (i.e., a polynomial where the degree of each variable in each term is either 0 or 1), e.g.,

$$x \oplus y = x + y - 2xy.$$

(Note that here ‘+’ denotes regular addition in the real numbers.) We can generalize this expression to decompose an expression of  $N$  parities into a multilinear polynomial:

$$x_1 \oplus \cdots \oplus x_N = - \sum_{\vec{y} \neq \vec{0}} (-2)^{|\vec{y}|-1} x_1^{y_1} \cdots x_N^{y_N}. \quad (1)$$

Note that the weight of a degree- $k$  term is  $2^{k-1}$ . This means that if we had a phase polynomial  $\phi$  where the smallest constant in its XOR form is  $2\pi/2^k$ , then all the terms in its multilinear form of degree greater than  $k$  will have a weight that is an integer multiple of  $2\pi$ , and hence can be ignored. In the example above, when we write  $e^{i\pi(x+y+x\oplus y)}$  in multilinear form we get  $e^{i\pi(2x+2y-2xy)}$ , so that it only contains expressions that are multiples of  $2\pi$ .

In particular, if we have a circuit of CNOT and T gates only (i.e.,  $\alpha = \pi/4$ ), the multilinear phase polynomial involves terms of degree at most 3, after having removed all the terms leading to multiple of  $2\pi$ . Hence, there is a one-to-one correspondence between  $N$ -qubit diagonal CNOT + T circuits and multilinear polynomials of the form

$$\phi(x_1, \dots, x_N) = \frac{\pi}{4} \left( \sum_i a_i x_i + 2 \sum_{i < j} b_{ij} x_i x_j + 4 \sum_{i < j < k} c_{ijk} x_i x_j x_k \right), \quad (2)$$

where  $a_i \in \{0, \dots, 7\}$ ,  $b_{ij} \in \{0, \dots, 3\}$  and  $c_{ijk} \in \{0, 1\}$ .

We can now check whether two diagonal CNOT + T circuits implement the same unitary by converting them to the multilinear phase polynomial representation of Eq. 2. However, since we are considering Clifford operations to be free, we only need to check whether two CNOT + T circuits are equal up to Clifford operations.

**Symmetric 3-tensors.** The multilinear representation corresponds directly to a circuit of T, CS and CCZ gates: each  $a_i x_i$  term is implemented by  $a_i$  T gates acting on the  $i$ th qubit; each  $b_{ij} x_i x_j$  term corresponds to  $b_{ij}$  CS gates on qubits  $i$  and  $j$ ; and each  $c_{ijk} x_i x_j x_k$  term corresponds to one CCZ gate on qubits  $i$ ,  $j$  and  $k$  if  $c_{ijk} = 1$ . Each of these terms only corresponds to a non-Clifford operation if the constant  $a_i$ ,  $b_{ij}$  or  $c_{ijk}$  is odd. Hence, to check whether two diagonal CNOT + T circuits implement the same unitary up to Clifford operations, we can calculate their multilinear polynomials in Eq. 2 and take modulo 2 of their coefficients. That is, two CNOT + T circuits are equal up to Clifford operations if and only if they have the same polynomial (after taking modulo 2 of their coefficients). All this information about the multilinear polynomial can then be captured in a single symmetric 3-tensor  $\mathcal{T}$  with entries in  $\{0, 1\}$ . Namely, we make the correspondence as follows: for  $i < j < k$  an entry  $\mathcal{T}_{ijk} = 1$  if we have  $c_{ijk} = 1$  in the corresponding polynomial  $\phi$ ; for  $i < j$ ,  $\mathcal{T}_{ijj} = 1$  if  $b_{ij} = 1$ ; and for any  $i$ , we have  $\mathcal{T}_{iii} = 1$  if  $a_i = 1$ .

**Rank of a tensor.** We can write a parity expression like  $x_1 \oplus x_3$  as a dot product with a vector  $\vec{y} = (1, 0, 1)$  via  $\vec{y} \cdot \vec{x} = y_1 x_1 \oplus y_2 x_2 \oplus y_3 x_3$ , where we take the value of the dot product to be modulo 2 and the ones in  $\vec{y}$  indicate which variables are part of the parity. Now, take an XOR phase polynomial consisting of a single term  $e^{i \frac{\pi}{4} \vec{y} \cdot \vec{x}}$ . We can also write this as  $e^{i \frac{\pi}{4} x_{a_1} \oplus \dots \oplus x_{a_k}}$  where the indices  $a_k$  indicate the positions wherer  $y_i = 1$ . Using Eq. 1 to decompose this polynomial into multilinear form, we get all combinations of the terms  $x_{a_i}$ ,  $2x_{a_i} x_{a_j}$  and  $4x_{a_i} x_{a_j} x_{a_k}$  —for all the variables  $x_i$  where  $y_i = 1$ . Hence, we set the corresponding symmetric 3-tensor  $\mathcal{T}_{ijk}$  as  $\mathcal{T}_{ijk} = y_i y_j y_k$ . This is then a *rank-one* symmetric tensor, as it is built out of a single vector  $\vec{y}$ . Let such a rank-one tensor be denoted as  $\mathcal{T}_{\vec{y}}$ . Any rank-one tensor is defined by a vector  $\vec{y}$ , and hence if a symmetric 3-tensor built from a phase polynomial has rank-one, then it corresponds to a single XOR term.

The translation from the XOR form into the 3-tensor is linear in the XOR terms. Hence, if the phase polynomial is a sum of parity terms,  $\{\vec{y}^1 \cdot \vec{x}, \vec{y}^2 \cdot \vec{x}, \dots, \vec{y}^k \cdot \vec{x}\}$ , then its corresponding symmetric 3-tensor is  $\mathcal{T} = \mathcal{T}_{\vec{y}^1} + \dots + \mathcal{T}_{\vec{y}^k}$ , where again the summation is under modulo 2. Conversely, each symmetric 3-tensor can be *decomposed* in this manner. The *rank* of the tensor is the number of terms in this decomposition. Thus, if we have a symmetric 3-tensor, finding a rank- $R$  decomposition corresponds to finding a set of  $R$  XOR parity terms that result in the same tensor, which hence implement the same unitary up to Clifford operations. Given that implementing the unitary matrix corresponding to a single parity phase requires one T gate, the T-count of this circuit is then exactly equal to the rank of the decomposition.

Therefore, we have reduced the problem of T-count optimization of CNOT + T circuits to finding Waring decompositions of symmetric  $N \times N \times N$  3-tensors with elements in  $\{0, 1\}$ .

## A.2 Quantum Chemistry

Due to the exponential computational cost associated with solving the Schrödinger equation for strongly correlated many-electron systems, state-of-the-art classical quantum chemistry methods struggle to accurately simulate strongly correlated molecules [44]. Quantum computers, in theory, can handle these calculations more efficiently, due to the logarithmic scaling of qubit number with system size. The FeMoco molecule, which is the active site in the nitrogenase enzyme responsible for nitrogen fixation, presents a compelling use case for quantum computing in strongly correlated quantum chemistry, due to its highly complex electronic structure [45]. The primary function of nitrogenase is to catalyze the conversion of atmospheric nitrogen (breaking a strong triple bond) at room temperature, into ammonia. Synthetically this is done via the Haber process which is incredibly energy intensive. The FeMoco molecule contains multiple atoms, including iron and molybdenum.

To understand complex reaction pathways such as those in FeMoCo one must first calculate the ground state energy of a molecule at a particular geometry. Of the techniques for fault-tolerant quantum computation of molecular ground states, the current most efficient method is the *linear combinations of unitaries* (LCU) method combined with *qubitization* for phase estimation, which leads to a linear T gate complexity in the outcome precision [33]. This can be further improved with Coulomb operator preprocessing that exploits sparsity [48] or the use of tensor hyper-contraction approaches [46]. Furthermore, beyond the Born-Oppenheimer approximation of fixed nuclei, a first quantized plane wave framework has been proposed as the optimal for molecules [64]. This approach has been extended to be used with pseudo potentials for simulating materials. Furthermore, these qubitized phase estimation techniques have been used to calculate molecular observables when combined with quantum signal processing [65].

The rest of this section assumes prior knowledge of the standard mathematical formulation of quantum computing and quantum algorithms. See de Wolf [66, Sections 4 & 9] for a more gentle introduction and Bauer et al. [67] for a more comprehensive reference on the applicability of quantum algorithms in chemistry.

**Quantum phase estimation.** The typical way to calculate ground state energies is to exploit the relation of a unitary matrix acting on its eigenvector  $|k\rangle$ , which when applied to a mixture of eigenstates  $|\psi\rangle = \sum_k c_k |k\rangle$ , gives a superposition

$$\langle\psi|U|\psi\rangle = \sum_j |c_k|^2 e^{i\phi_k} \langle k|k\rangle.$$

where  $e^{i\phi_k}$  are the eigenvalues of  $U$  (and we call  $\phi_k$  the eigenphases).

The canonical phase estimation algorithm is shown in Figure 9. The ancilla register is prepared in the Hadamard basis, then phase-kickback of controlled unitaries acting on their eigenbasis  $U|k\rangle = e^{i\phi_k}|k\rangle$  is used to put the powers of eigenphases into the Fourier basis on the ancilla register. The eigenphases are then extracted into the computational basis from the Fourier basis using the inverse quantum Fourier transform. Readout of the ancilla bits gives the eigenphases in fixed-point binary representation. The eigenstates with the dominant initial overlap will have their eigenphases obtained with the largest probability. Therefore it is required that the initial state must have dominant overlap with the state of interest. Generating initial states with this property is an unresolved problem in quantum chemistry and has been discussed by Lee et al. [68].

In quantum chemistry applications, we encode the energies of the eigenstate  $|k\rangle$  of the Hamiltonian describing the chemical system into the phase  $\phi_k$  using the qubitized quantum walk unitary from Eq. 4 (see below). Qubitized quantum phase estimation [33] applies a controlled quantum-walk operator as opposed to a

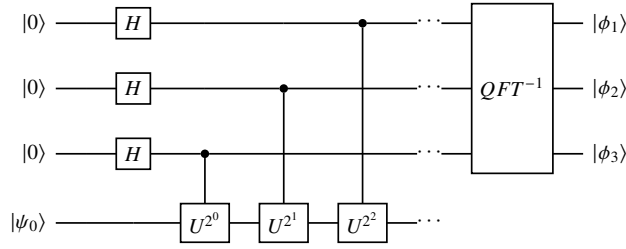


**Figure 9:** Canonical quantum phase estimation.

controlled time-evolution operator, where the Hamiltonian  $H$  of the system is encoded in the quantum walk operator  $W = e^{i \arccos(H)\hat{Y}}$ , where  $\hat{Y}$  is the Pauli  $Y$  operator applied to each eigenvector independently. The eigenphases of this walk operator are proportional to the Hamiltonian eigenvalues  $E_k$  and can be extracted when applied to eigenstates  $|k\rangle$  of the Hamiltonian. Consider any state  $|\psi\rangle = \sum_k c_k |k\rangle$ , then:

$$\langle \psi | W | \psi \rangle = \langle \psi | e^{i \arccos(H)\hat{Y}} | \psi \rangle = \sum_k |c_k|^2 e^{\pm i \arccos(E_k)} \langle k | k \rangle.$$

A naive implementation of the controlled quantum walk circuit  $W$  is shown in Figure 7. Its complexity can be improved by using the techniques employed by Babbush et al. [33], which exploit adjacent cancellation of reflection operators and a different initial ancilla state.

**Linear combination of unitaries.** The  $U_{LCU}$  operator is a block encoding the Hamiltonian of interest, describing the molecule at a given geometry. It uses two registers, a state register and a prepare register. The block encoding is indexed by the unique bit strings of the PREPARE register, it can be thought of as there being a state block for each PREPARE register row and column bit strings.

A Hamiltonian operator can be decomposed into a LCU by

$$H = \sum_{\ell=0}^{L-1} \alpha_{\ell} H_{\ell},$$

where  $H_{\ell}$  is a unitary matrix and  $\alpha_{\ell}$  a linear expansion coefficient. We can assume  $\alpha_{\ell}$  to be a real positive number, since any complex phases in the coefficients can be absorbed into  $H_{\ell}$ . The LCU circuit primitives were first introduced by Childs and Wiebe [69]. The operator  $H$  is encoded into a block of a larger unitary matrix  $U_{LCU}$ , and it is accessed by projecting into the block via post-selection – that is, we measure the qubits defining the block structure, and the encoding succeeds when this returns zero. To ensure the overall matrix  $U_{LCU}$  is unitary, the operator is re-scaled by  $|\alpha|$ , its  $L_1$ -norm, i.e.,

$$U_{LCU} = \begin{pmatrix} \frac{H}{|\alpha|} & * \\ * & * \end{pmatrix}, \quad \text{where } |\alpha| = \sum_{\ell} |\alpha_{\ell}|.$$

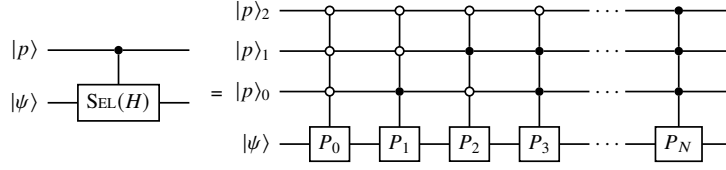


**Figure 10:** SELECT circuit implementing  $\sum_{\ell} |\ell\rangle\langle\ell| \otimes P_{\ell}$ .

The Hamiltonian is encoded into a quantum circuit via two oracles:  $\text{SELECT}(H)$  and  $\text{PREPARE}(\alpha)$  which encode the unitaries  $H_{\ell}$  and the coefficients  $\alpha_{\ell}$  respectively. The  $\text{PREPARE}(\alpha)$  transforms the all zeros state of the control register to a state  $|p\rangle$  (with positive real amplitudes) defined by the given coefficients in Eq. 3,

$$\text{PREPARE}(\alpha) : |0\rangle \mapsto \sum_{\ell=0}^{L-1} \sqrt{\frac{\alpha_{\ell}}{|\alpha|}} |\ell\rangle = \begin{bmatrix} \sqrt{\frac{\alpha_0}{|\alpha|}} & \cdot & \dots \\ \sqrt{\frac{\alpha_1}{|\alpha|}} & \cdot & \dots \\ \vdots & \ddots & \dots \\ \sqrt{\frac{\alpha_{k-1}}{|\alpha|}} & \cdot & \dots \end{bmatrix} \quad (3)$$

A leading fault-tolerant primitive was proposed by Low et al. [70]. The signs and phases of the coefficients are pulled into the SELECT.

It must be noted that upon an action of the SELECT, an orthogonal complement  $|p_{\perp}\rangle$  will also be generated, which leads to success probabilities (of the block-encoding) of less than 1. The SELECT oracle is typically a multi-controlled unitary matrix that applies the Hamiltonian terms to the state register via a multi-control for each term, indexed by a unique PREPARE register bit string. A fault tolerant approach was proposed by Babbush et al. [33] built upon Gidney's work [31]. The multi-control multiplies the weighting coefficient from the PREPARE to the Pauli for that bit string and applies the weighted Pauli to the state register. The SELECT oracle is shown in Figure 10 and given by

$$\text{SELECT}(H) := \sum_{\ell=0}^{L-1} |\ell\rangle\langle\ell| \otimes H_{\ell}$$

While any operator can in principle be written as a linear combination of unitary matrices, second quantized Hamiltonians in the Pauli representation are naturally expressed in this framework. The  $\text{SELECT}(H)$  and  $\text{PREP}(\alpha)$  oracles can be combined to create a probabilistic circuit for acting on an arbitrary quantum state  $|\psi\rangle$  with an operator  $\frac{H}{|\alpha|}$ ; this is shown in Figure 11.

The operation  $\frac{H}{\alpha}|\psi\rangle$  is successful if a measurement on the prepare register returns  $|\bar{0}\rangle$ . The success probability is related to the closeness of  $H$  to being unitary and the initial state overlap,

$$P_{\text{success}} = \frac{1}{|\alpha|^2} \langle \psi | H^{\dagger} H | \psi \rangle$$

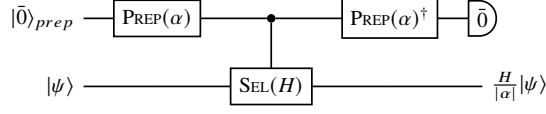


**Figure 11:** LCU Circuit acting on an arbitrary quantum state  $|\psi\rangle$  with a rescaled operator  $\frac{H}{|\alpha|}$ , when a successful post-selection occurs.

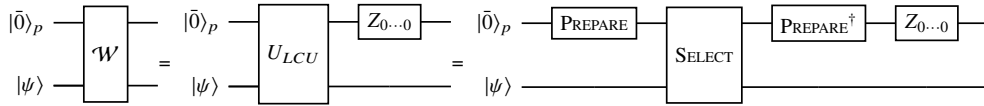
The  $L_1$ -norm of the operator has a significant effect on the success probability and this is the dominant factor in the complexity results analysis. Therefore the majority of work on trying to improve the complexity of LCU methods typical aiming to reduce the  $L_1$ -norm of the operator.

**Qubitization.** First proposed by Low and Chuang [71], qubitization is a powerful method allowing one to implement polynomials of block encoded operators. In block encoding methods we are typically only interested in the PREPARE  $|0 \dots 0\rangle\langle 0 \dots 0|$  block of the unitary matrix where the Hamiltonian is encoded. The rest of the rows and columns of the unitary matrix are referred to as the orthogonal complement,  $|0 \dots 0_\perp\rangle$ .

$$U_{LCU} = \begin{pmatrix} |0 \dots 0\rangle\langle\psi| & |0 \dots 0_\perp\rangle\langle\psi| \\ H & * \\ * & * \end{pmatrix} \begin{pmatrix} |0 \dots 0\rangle\langle\psi| \\ |0 \dots 0_\perp\rangle\langle\psi| \end{pmatrix} = \bigoplus_k \begin{pmatrix} \lambda_k & \sqrt{1 - \lambda_k^2} \\ \sqrt{1 - \lambda_k^2} & -\lambda_k \end{pmatrix} \begin{pmatrix} |0 \dots 0\rangle\langle k| \\ |0 \dots 0_\perp\rangle\langle k| \end{pmatrix}.$$

In the eigenbasis  $|\psi\rangle = \sum_k \lambda_k |k\rangle$  the  $U_{LCU}$  becomes a direct sum of  $2 \times 2$  blocks indexed on each eigenvector. Where the orthogonal complement  $|0 \dots 0_\perp\rangle$  of the prepare register is given an arbitrary vector which just has to exist to generate the qubitized  $2 \times 2$  subspace via some Gram-Schmidt projection. We can then turn this into a quantum walk operator by applying a reflection, which is typically implemented as a all-0 CZ gate with a minus phase,

$$W = \bigoplus_k \begin{pmatrix} 1 & 0 \\ 0 & -1 \end{pmatrix} \begin{pmatrix} \lambda_k & \sqrt{1 - \lambda_k^2} \\ \sqrt{1 - \lambda_k^2} & -\lambda_k \end{pmatrix} = \bigoplus_k \begin{pmatrix} \lambda_k & \sqrt{1 - \lambda_k^2} \\ -\sqrt{1 - \lambda_k^2} & \lambda_k \end{pmatrix}.$$



Therefore, powers of the quantum walk operator take the form of increments of an  $R_y(\arccos(\lambda_k))$  rotation in the  $2 \times 2$  sub-spaces of  $\{|0 \cdots 0\rangle|k\rangle, |0 \cdots 0_\perp\rangle|k\rangle\}$ . These rotation matrices can be interpreted in terms of the Chebyshev polynomials of the first  $T_d(\lambda_k)$  and second  $U_d(\lambda_k)$  kind:

$$W^d = \bigoplus_k \begin{pmatrix} \cos(d\theta_k) & \sin(d\theta_k) \\ -\sin(d\theta_k) & \cos(d\theta_k) \end{pmatrix} = \bigoplus_k \begin{pmatrix} T_d(\lambda_k) & \sqrt{1-\lambda_k^2}U_{d-1}(\lambda_k) \\ -\sqrt{1-\lambda_k^2}U_{d-1}(\lambda_k) & T_d(\lambda_k) \end{pmatrix} = \begin{pmatrix} T_d(H) & \cdot \\ \cdot & \cdot \end{pmatrix}$$

The phase of this operator can be found in the same way as traditional phase estimation using a controlled quantum-walk:

$$\langle \psi | W | \psi \rangle = \langle \psi | e^{i \arccos(H) \hat{Y}} | \psi \rangle = \sum_k |c_k|^2 e^{\pm i \arccos(E_k)} \langle k | k \rangle \quad (4)$$

This operation is the compilation target for the quantum chemistry section of this work.

## B Baselines

Methods for T-count optimization are broadly divided into two camps: those that treat all non-Clifford phase gates equivalently, and those that utilize specific optimizations for T gates. In the algorithms in the first category [e.g., 14, 17, 19, 37], non-Clifford rotation gates are treated as distinct black boxes, without any knowledge of transformations relating them, except that they can be merged together to reduce the number of gates. While limited in this way, they also have the ability to optimize all circuits, regardless of the gates used, and in particular they can optimize circuits containing Hadamard gates.

By contrast, algorithms in the second category [e.g., 16, 18, 23] are based (either directly or indirectly) on the representation of CNOT+T circuits as Waring decompositions of the signature tensor, as they are considered in AlphaTensor-Quantum. These generally perform better on such circuits than the black-box methods. However, since they cannot optimize around Hadamard gates, it is beneficial to first apply a black-box optimizer that can do so [34].

To obtain the baseline T-count for the circuit benchmarks used in this work, we applied the phase-teleportation algorithm of Kissinger and van de Wetering [19] followed by compiling the circuits to the Waring decomposition using the steps detailed in Appendix C.1. Then we apply TODD [16] and STOMP [23] and take the output with better T-count. (For STOMP, we took the best of twenty runs.) For the standard arithmetic benchmarks (i.e., the non-split circuits), we compared against the published T-count numbers and took whichever was better.

We chose phase-teleportation because it was shown to be essentially optimal for reducing T-count in the black-box setting [72], and TODD/STOMP were chosen because they consistently outperform other methods [18] in published benchmarks. While TODD and STOMP both have methods to compile Clifford+T circuits to a Waring decomposition, we opt to use the method in Appendix C.1 as it includes a more recent and better performing method from Vandaele et al. [34].

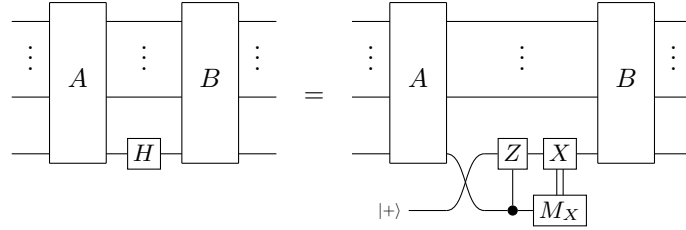
## C Method Details

### C.1 Compilation of the Quantum Circuits

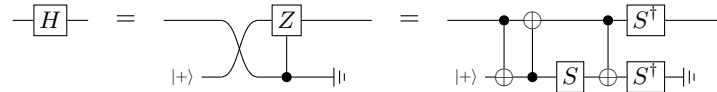
To obtain signature tensors suitable for optimization with AlphaTensor-Quantum from quantum circuits, we proceed as follows:

1. First, we express the input circuit over the  $\{H, Z, S, T, \text{CNOT}\}$  gate set.
2. We apply the phase-teleportation optimization algorithm of Kissinger and van de Wetering [19] to reduce the initial number of T gates as much as possible. As discussed in Appendix B, this is particularly beneficial because phase-teleportation can optimize around Hadamard gates.
3. We rewrite the circuit to contain as few internal Hadamard gates as possible, using the algorithm of Vandaele et al. [34]. A Hadamard gate is internal if there are T gates between it and both the beginning and end of the circuit that it cannot commute with (for example, in the sequence  $HTHTH$  the second Hadamard is internal but the first and third ones are not).
4. We split the circuit  $U$  into alternating blocks of Clifford circuits  $B_i$  and circuits  $A_i$  containing only CNOT and phase gates, such that  $U = B_m A_{m-1} B_{m-1} \cdots A_1 B_1$ . We accomplish this by scanning the circuit from left to right, collecting as many Clifford gates as possible into the first block  $B_1$  until we encounter a T gate. After this, we collect gates into the block  $A_1$  until we encounter a Hadamard gate. Then we switch to collecting Clifford gates into block  $B_2$ , etc. We proceed in this way until the whole circuit has been consumed.
5. We apply the Hadamard gadgetization process of Heyfron and Campbell [16] to remove all internal Hadamard gates by replacing them with ancilla and Clifford gates. In Section 3.1, if this process generates more than 60 qubits, we take the output of the previous step and use the technique in Appendix C.2 to split the circuit into smaller sections, and we repeat this compilation process on each. We discuss Hadamard gadgetization in further detail below.
6. At this point we can partition the circuit into the form  $U = U_3 U_2 U_1$  where  $U_1$  and  $U_3$  contain Clifford gates and non-internal Hadamard gates, and  $U_2$  contains only CNOT and phase gates. Let  $C$  be the circuit formed by taking just the CNOT gates in  $U_2$ , then consider the transformation  $U = U_3' U_2' U_1 = (U_3 C)(C^\dagger U_2) U_1$ . Now,  $U_2'$  is a diagonal operator. Let  $V$  be the circuit formed by removing all T gates from  $U_2'$  and  $W$  be the circuit formed by removing all S and Z gates from  $U_2'$ . Then  $V$  is Clifford,  $W$  contains only CNOT and T gates, and it can be shown that  $U_2' = VW$ , so  $U = (U_3 CV) W U_1$ . Therefore, all the non-Clifford components of the original circuit  $U$  is now contained within  $W$ .
7. We map  $W$  to a Waring decomposition of the signature tensor as follows. Suppose  $W$  contains  $R$  T gates and  $N$  qubits, then let  $A$  be a  $N \times R$  matrix in  $\mathbb{F}_2$ . For the  $i$ th T gate in  $W$ , set  $A_{ji} = 1$  if it appears on the  $j$ th qubit, and  $A_{ji} = 0$  otherwise. Scan over  $W$  from left to right: for each CNOT gate with control  $a$  and target  $b$ , if there are any T gates to its right, then let  $i'$  be the corresponding column of  $A$  and set  $A_{ai} \leftarrow A_{ai} + A_{bi}$  for all  $i' \leq i \leq R$ . After all CNOT gates have been processed,  $A$  will be a Waring decomposition of the signature tensor of  $W$ , which we can calculate as  $\mathcal{T}_{ijk} = \sum_{m=1}^R A_{im} A_{jm} A_{km}$ . This is then ready to be optimized with AlphaTensor-Quantum. Overall, this procedure is the same as the phase polynomial method in Section 5.1, but phrased in terms of matrices.

**Hadamard gadgetization.** To remove the internal Hadamard gates from a circuit, we can use the Hadamard gadgetization method of Heyfron and Campbell [16]. In this method, each Hadamard gate is replaced with the following gadget circuit, consisting of an ancilla, Clifford gates, measurements, and classically-controlled gates (here,  $A$  and  $B$  represent the rest of the circuit):



However, in this implementation, we assume that the measurement always returns zero. Therefore, the corresponding gadget implementation is as follows (additionally rewritten to our target gate set):



This is justified in that it does not change the non-Clifford behaviour of a circuit—in fact, the classically controlled X gate correction factor can be translated into a controlled Clifford operator at the end of the circuit [16, 23], hence the T-count is unchanged by this assumption. Because computing these correction factors is complicated, and existing quantum circuit representations have poor support for classically-controlled operations; this decision was also made for the implementations of both TODD [16] and STOMP [23]. Since fault-tolerant quantum computing is still a number of years away from practical implementation, we argue that this is acceptable at this stage.

**Reconstructing optimized circuits.** In order to reconstruct an optimized form  $W'$  of the diagonal circuit  $W$  computed above, we can follow the steps in Appendix C.3 given a new Waring decomposition of the signature tensor  $\mathcal{T}$ . With  $W'$ , we can recompose the original circuit  $U = (U_3CV)WU_1$ . However, note that  $W'$  may differ from the original  $W$  by a diagonal Clifford factor, so it must be corrected. This factor can be computed, given the original and optimized Waring decompositions along with  $V$ , by considering the difference between the signature tensors over  $\mathbb{Z}$  rather than  $\mathbb{F}_2$ —see Heyfron and Campbell [16] for more details. As discussed above, in this process we discarded the classically-controlled Clifford gates incurred during Hadamard gadgetization. It is possible in principle (and computationally easy) to take these into account—see de Beaudrap et al. [23] for more details and Heyfron and Campbell [16] for the general method. Since in this work we only determine the optimized T-count rather than reconstructing the circuit, we do not need to implement either of these steps.

## C.2 Splitting Larger Quantum Circuits

During the compilation process, each quantum circuit  $U$  is split into a list of blocks alternating between circuits  $A_i$  containing CNOT and phase gates, and Clifford circuits  $B_i$ , i.e.,

$$U = B_m A_{m-1} B_{m-1} \cdots A_2 B_2 A_1 B_1.$$

For most circuits, we can then proceed with Hadamard gadgetization of the  $B_i$  blocks as described above. However, for some circuits, this would result in a circuit with too many qubits. Hence, we choose some boundaries  $1 = j_1 < j_2 < \cdots < j_k = m$  to break up the circuit into a set of subcircuits:

$$U_i = A_{j_{i+1}-1} B_{j_{i+1}-1} \cdots A_{j_i} B_{j_i} \text{ where } U = B_m U_k \cdots U_1.$$

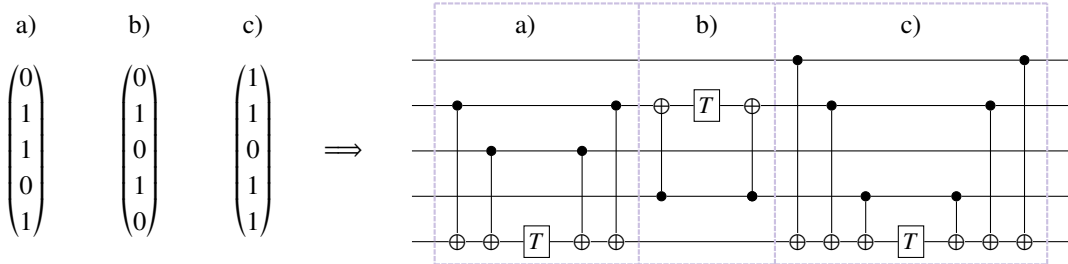
We want to minimize  $k$  in order to maximize the number of T gates that can be considered together in each block. To do this, we use a random-greedy algorithm: fix a threshold  $t$  on the maximum number of qubits allowed in any subcircuit (e.g., 60), and initially let  $j_i = i$  so that  $k = m$ . For any consecutive pair  $U_i$  and  $U_{i+1}$ , we consider them to be *compatible* if

$$|\text{supp } U_i \cup \text{supp } U_{i+1}| + \sum_{j_i < n < j_{i+2}} |B_n|_H \leq t,$$

where  $\text{supp } U_i$  is the set of qubits used by gates on  $U_i$ , and  $|C|_H$  is the number of Hadamard gates in  $C$ . While there is any compatible pair remaining, pick one at random and set  $j_n \leftarrow j_{n+1}$  for  $n \geq i+1$  and  $k \leftarrow k-1$ . In this way, we merge consecutive compatible pairs until there are only a few blocks remaining, and combining any two of them would result in too many qubits being generated. We repeat this process 1 000 times and take the run that results in the smallest value of  $k$ . We can then treat each  $U_i$  as its own target circuit, processing it back through the compilation pipeline, and optimizing it with AlphaTensor-Quantum. To composite the final circuit we combine the  $U_i$  along with the Clifford circuit  $B_m$  to form  $U = B_m U_k \cdots U_1$ .

## C.3 Gadgetization

The conversion of phase-gadget circuits to Waring decompositions of the signature tensor as described in Appendix C.1 can be inverted to obtain a phase-gadget circuit from a decomposition by placing a CNOT-fanout structure conjugating a T gate for each factor, where the target corresponds to some non-zero entry in the factor, and the controls are on every other non-zero entry. For example:



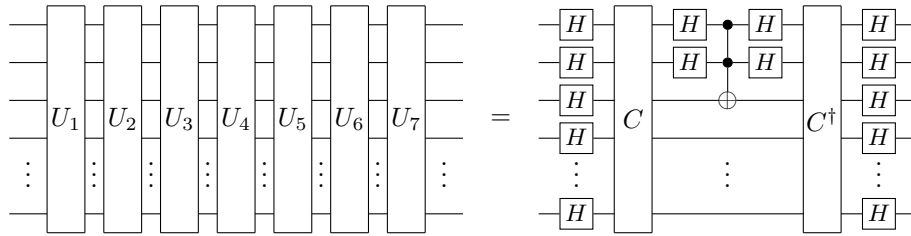
Note that this is not optimal with respect to the number of CNOT gates, and many strategies have been developed to improve this [73–75]. In this work we ignore the cost of Clifford gates, and so do not attempt

to optimize this step. If we are constrained to CNOT+T circuits, this method is optimal in terms of T gates, but some patterns of factors can be implemented with fewer non-Clifford resources if we make use of ancilla qubits, measurements, and classically-controlled Clifford gates.

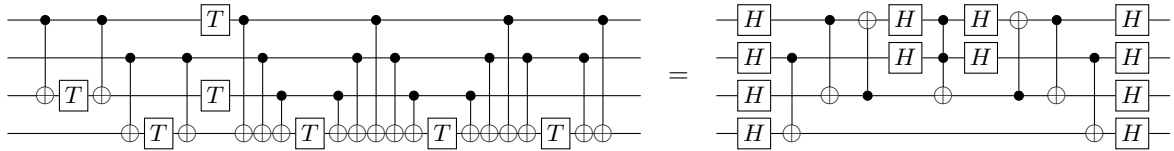
In particular, suppose we have factors  $u^{(1)} \cdots u^{(7)}$  such that  $u^{(1)}$ ,  $u^{(2)}$  and  $u^{(3)}$  are linearly independent, and the following equations are satisfied:

$$\begin{aligned} u^{(4)} &= u^{(1)} + u^{(2)} \\ u^{(5)} &= u^{(1)} + u^{(3)} \\ u^{(6)} &= u^{(1)} + u^{(2)} + u^{(3)} \\ u^{(7)} &= u^{(2)} + u^{(3)} \end{aligned}$$

where addition is considered elementwise over  $\mathbb{F}_2$ . We call such patterns *Toffoli gadgets*. They can be implemented using a single Toffoli gate conjugated by CNOT and Hadamard gates as follows,



where  $U_i$  denotes the CNOT-fanout circuit given above for factor  $u^{(i)}$ , and  $C$  is a CNOT circuit such that  $C|u^{(1)}\rangle = |100\dots\rangle$ ,  $C|u^{(2)}\rangle = |010\dots\rangle$ ,  $C|u^{(3)}\rangle = |001\dots\rangle$ . This can be proven by considering this circuit in the sum-over-paths formalism [63]. For example:

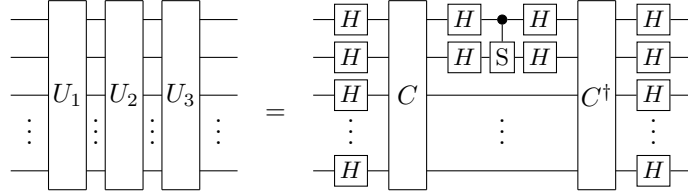


Since Toffoli gates can be implemented efficiently using either four T gates or a CCZ magic state which using state of the art factories costs the same as two T gates (see Figure 12), each Toffoli gadget can be implemented more efficiently than the seven T gates required to represent it as a phase-gadget circuit.

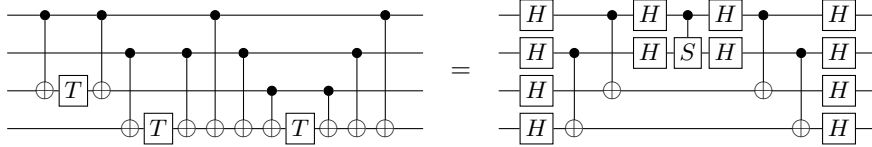
Because  $u^{(1)}$ ,  $u^{(2)}$ ,  $u^{(3)}$  are linearly independent, such a circuit  $C$  must exist. To construct it, we first build an invertible matrix  $M$  over  $\mathbb{F}_2$  such that the first three columns of  $M$  are  $u^{(1)}$ ,  $u^{(2)}$ ,  $u^{(3)}$  respectively. The remaining columns of  $M$  can be computed as a basis for the kernel of the first three via Gaussian elimination. Then we can synthesize a CNOT circuit  $C$  such that  $C|x\rangle = |M^{-1}x\rangle$  using the Patel-Markov-Hayes algorithm. By definition, this must send  $|u^{(1)}\rangle$  to  $|100\dots\rangle$ , etc., as required. Therefore, to encourage Toffoli gadgets to be played by AlphaTensor-Quantum, we assign a positive reward to moves which complete a group. To identify when this happens, we set  $u^{(1)}$  to be the factor at step  $s - 6$ ,  $u^{(2)}$  to be the factor at step  $s - 5$ , and so

on, so that  $u^{(7)}$  is the last played action (at step  $s$ ).<sup>1</sup> Finally, to synthesize a quantum circuit from a Waring decomposition of the signature tensor, we apply this construction to any Toffoli gadgets that were identified by AlphaTensor-Quantum, and synthesize the remaining factors with the CNOT-fanout approach from above.

In the same way, we call groups of three factors  $u^{(1)}, u^{(2)}, u^{(3)}$  such that  $u^{(1)}$  and  $u^{(2)}$  are linearly independent and  $u^{(3)} = u^{(1)} + u^{(2)}$  *CS gadgets*. In this case, such a group can be implemented by a single CS gate conjugated by CNOT gates:



The CNOT circuit  $C$  is such that  $C|u^{(1)}\rangle = |10\dots\rangle$  and  $C|u^{(2)}\rangle = |01\dots\rangle$ , and it can be generated in exactly the same way as for the Toffoli gadget case. For example:



The central CS gate can be implemented using a CCZ magic state (see Figure 13), which costs the same as two T gates, and so the whole gadget can be implemented more efficiently than representing it as a phase-gadget circuit with three T gates. Note that in both of these gadgets, most of the Hadamard gates can be eliminated by commuting them with the CNOT gates in  $C$ .

## C.4 Neural Network Architecture

As shown in Figure 8a, the neural network has three main components: the torso, the policy head, and the value head.

The input to the neural network is formed from the current game state, which, at step  $s$  of TensorGame, is composed of a (residual) tensor  $\mathcal{T}^{(s)}$  and a list of all the previously played actions  $u^{(s')}$ , with  $s' < s$ . To form the input to the network, we only consider the last  $T = 20$  actions; specifically we stack them into a tensor of size  $N \times N \times T$ , where each  $N \times N$  slice is obtained by taking the outer product  $u^{(s')} \otimes u^{(s')}$ . This tensor is concatenated with  $\mathcal{T}^{(s)}$ , as well as with the output of a linear layer that takes as input a single scalar: the square root of the quotient between  $s$  and the maximum number of allowed moves, which is 250. Figure 14 shows an overview of the torso.

The concatenated inputs are first passed through a linear layer that maps from  $\mathbb{R}^{N+T+1}$  to  $\mathbb{R}^c$ , with  $c = 512$ . The output of this layer is passed through  $L = 4$  layers of symmetrized axial attention (see Figure 8b),

<sup>1</sup>Any permutation of the seven factors could be absorbed in  $C$  and therefore it would still correspond to a Toffoli gadget. Additionally, the seven factors do not need to be consecutive in order to form a Toffoli gadget. However we impose a specific ordering of the (consecutive) factors  $u^{(1)}, \dots, u^{(7)}$  for two reasons. First, the sequence of seven factors does not include the pattern of the CS gadget as a subsequence. Second, this makes it easier for the RL agent to automatically detect and exploit the gadgetization patterns.

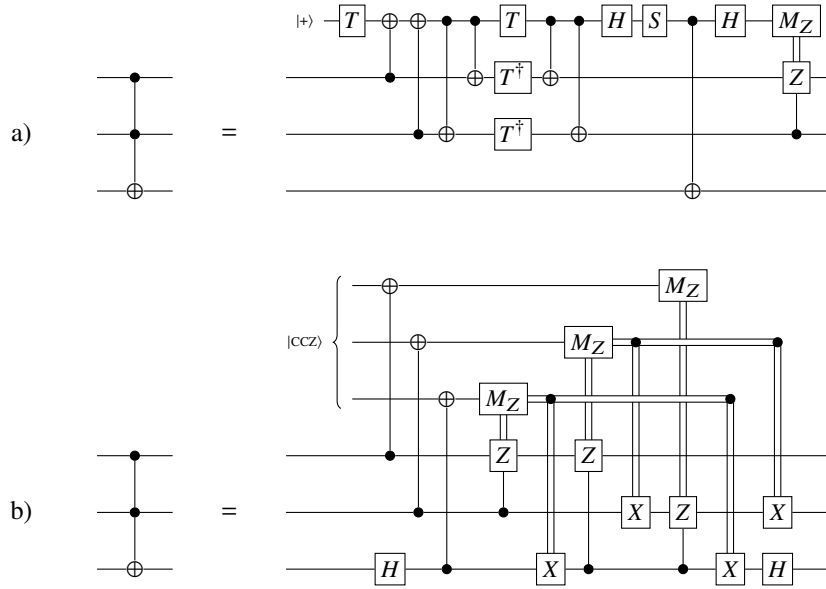


**Figure 12:** The Toffoli gate can be implemented efficiently using ancilla qubits, measurements, classically-controlled Clifford gates, and either four T gates (a) as in Jones [25], or a CCZ magic state (b) which are produced natively by the magic state factories of Gidney and Fowler [8] at a cost equivalent to two T gates.

which alternates self-attention operations with symmetrization layers. Each attention operation is depicted in Figure 15 and uses multi-head attention with 16 heads and head depth 32. The dense layer in Figure 15 consists in a feed-forward neural network with a single hidden layer that has twice as many hidden units as the input (and that applies the ReLU non-linearity).

Finally, the output of the torso is reshaped and passed to the policy and value heads (see Figure 14). The architecture of both the policy and value heads is taken from Fawzi et al. [24]. In particular, for the policy head, we use an autoregressive model that predicts  $\tilde{N}$  entries of  $u^{(s)}$  at a time, where  $\tilde{N}$  divides  $N$ . For instance, we use  $\tilde{N} = 10$  for the experiments from Section 3.1 for which  $N = 60$ , and  $\tilde{N} = 12$  for the experiments on unary iteration for which  $N = 72$ .

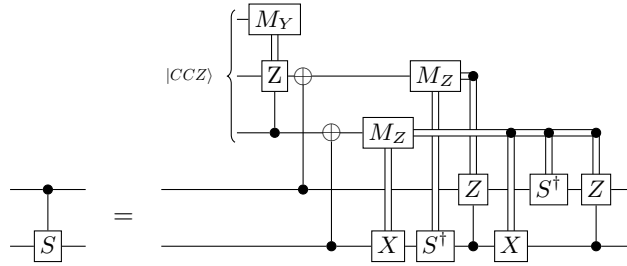


**Figure 13:** A CS gate can implemented efficiently [26, Appendix A] using ancilla qubits, measurements, classically-controlled Clifford gates and a CCZ magic state which is produced natively by the magic state factories of Gidney and Fowler [8] at a cost equivalent to two T gates.

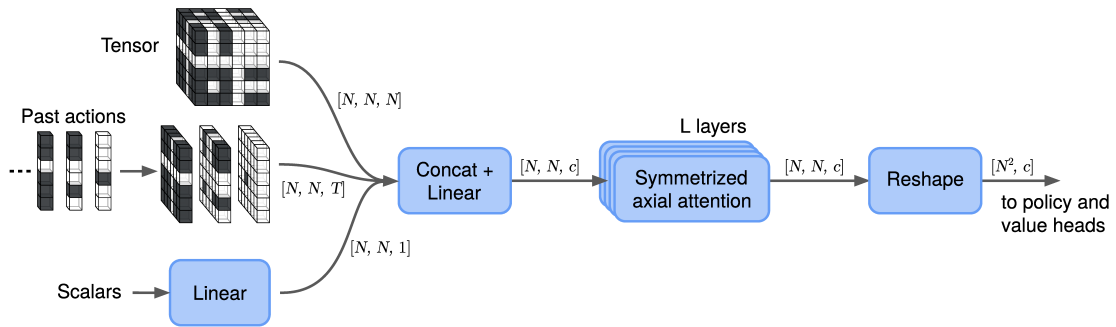


**Figure 14:** Overview of the neural network torso. Its main component is a stack of symmetrized axial attention layers.

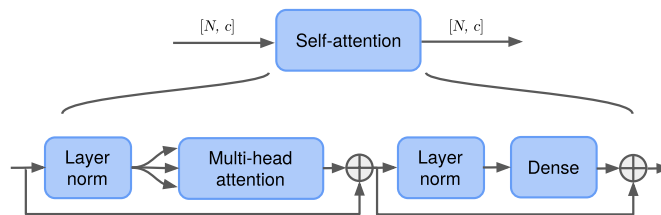


**Figure 15:** Overview of the self-attention operation. It features the standard components of a self-attention layer [60], including skip connections, layer normalization, multi-head attention, and a dense (fully connected) network with one hidden layer. When the input is a tensor of size  $N \times N \times c$ , the self-attention layer is applied independently over each row (or column) of the input.

## D Additional Results

### D.1 Additional Benchmark Circuits

The benchmark circuits  $\text{GF}(2^2)$ -mult and  $\text{GF}(2^3)$ -mult are derived from Cheung et al. [27] in the same way as the rest of the  $\text{GF}(2^m)$ -mult ( $m \geq 4$ ) series of circuits available from Amy [36], using the irreducible polynomials  $X^2 + X + 1$  and  $X^3 + X + 1$  respectively. We include them to complete the series, since  $m = 2$  is the smallest interesting instance ( $m = 1$  corresponds to a single Toffoli gate). For reference, the source code is given in OpenQASM 2.0 format as follows:

**Listing 1:**  $\text{GF}(2^2)$ -mult

```
OPENQASM 2.0;
include "qelib1.inc";
qreg a[2];
qreg b[2];
qreg c[2];
ccx a[1], b[1], c[0];
cx c[0], c[1];
ccx a[0], b[0], c[0];
ccx a[1], b[0], c[1];
ccx a[0], b[1], c[1];
```

**Listing 2:**  $\text{GF}(2^3)$ -mult

```
OPENQASM 2.0;
include "qelib1.inc";
qreg a[3];
qreg b[3];
qreg c[3];
ccx a[1], b[2], c[0];
ccx a[2], b[1], c[0];
ccx a[2], b[2], c[1];
cx c[1], c[2];
cx c[0], c[1];
ccx a[0], b[0], c[0];
ccx a[1], b[0], c[1];
ccx a[0], b[1], c[1];
ccx a[2], b[0], c[2];
ccx a[1], b[1], c[2];
ccx a[0], b[2], c[2];
```

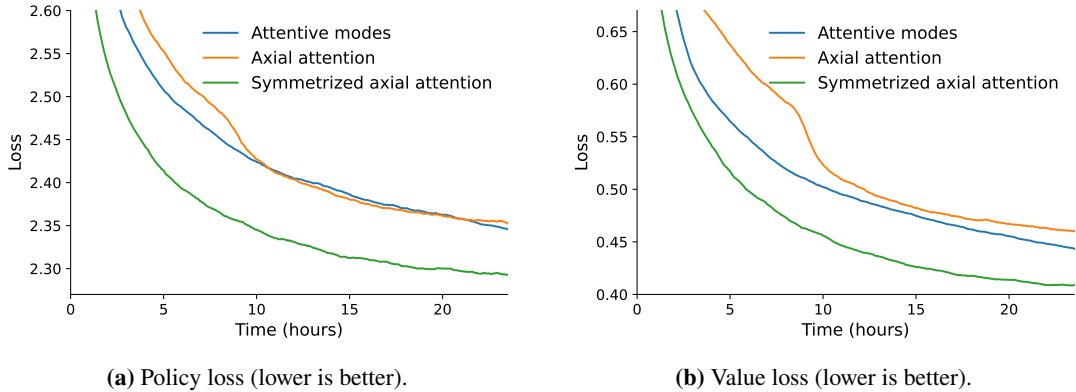
### D.2 Benchmarks Circuits with a Larger Number of Qubits

Table 3 reports the T-count obtained on the circuits from Section 3.1 that were split into sub-circuits (i.e., the ones marked with \* in Table 2), together with the T-count for each of the sub-circuits. For each sub-circuit, the baseline T-count was obtained as described in Appendix B.

### D.3 Neural Network Ablations

Here we compare different architectures for the torso of the neural network (see Section 5.2 and appendix C.4).

**Comparison across architectures.** We first compare the following: (i) *attentive modes* [24], which uses attention operations across pairs of modes of the input tensor; (ii) *axial attention* [61], which we recover when we eliminate the symmetrization layers from our architecture in Figure 8b; and (iii) *symmetrized axial attention*, which is the architecture that we introduce in Section 5.2, featuring symmetrization layers.



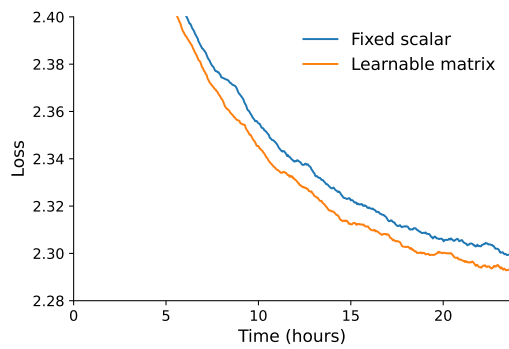
**Figure 16:** Comparison of different architectures for the torso of the neural network on a supervised experiment on  $30 \times 30 \times 30$  tensors. Symmetrized axial attention performs best. The reported policy loss is the average cross-entropy loss for the first step of the autoregressive model. (For better visualization, all curves have been smoothed using an average moving window of size 20.)

We run each architecture on a *supervised* experiment with synthetic data only (i.e., a system without actors), using tensors of size  $N = 30$ , and compare the loss that they achieve. For each of the methods, we set the number of layers  $L = 4$ . For axial attention and symmetrized axial attention, this means 8 (batched) attention operations with  $N$  tokens each; for attentive modes, this means 12 (batched) attention operations with  $2N$  tokens each. Therefore, we expect the architecture of Fawzi et al. [24] to run slower, and in fact we verify that its runtime is about 2x that of the other architectures: attentive modes runs at about 6 iterations per second, while axial attention and symmetrized axial attention complete 11.8 and 11.4 iterations per second, respectively.

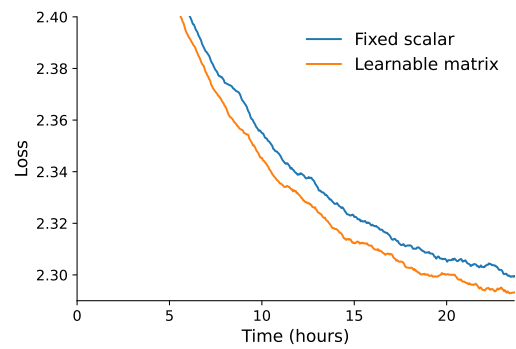
We report in Figure 16 the training loss from each head of the neural network (the loss on a test set performs similarly). While axial attention and symmetrized axial attention run at approximately the same speed, the symmetrization layers bring a significant boost in performance. In contrast, although the architecture based on attentive modes performs almost as good as symmetrized axial attention if ran for longer, its decreased speed make it an impractical choice for AlphaTensor-Quantum (it also presents memory issues when applied on larger tensors).

**Comparison of symmetrization layers.** We now consider two different choices for the symmetrization layers. Recall that the symmetrization operation performs the operation  $X \leftarrow \beta \odot X + (1 - \beta) \odot X^T$ . We refer to the choice of  $\beta = \frac{1}{2}$  as *fixed scalar*, in contrast to letting  $\beta \in \mathbb{R}^{N \times N}$  be a *learnable matrix*.

We compare both versions of symmetrization in Figure 17, where we report the training loss. Using a learnable matrix provides a small improvement over a fixed scalar (both choices run at approximately the same speed of 11.4 iterations per second). Letting  $\beta$  be a learnable matrix increases the number of model parameters by a negligible fraction (e.g., in this scenario, it adds 3 600 parameters to a model of approximately 132.7 million parameters).



(a) Policy loss (lower is better).



(b) Value loss (lower is better).

**Figure 17:** Comparison of different versions of the symmetrization operation, on a supervised experiment on  $30 \times 30 \times 30$  tensors. Symmetrization layers with learnable parameters lead to some performance improvement. The reported policy loss is the average cross-entropy loss for the first step of the autoregressive model. (For better visualization, all curves have been smoothed using an average moving window of size 20.)

Circuit	#Qubits	Baselines	AlphaTensor-Quantum	
			Without gadgets	With gadgets
<b>8-bit adder</b>		<b>129 [16]</b>	139	<b>94</b> (33Tof + 28T)
block 1	31	50	<b>48</b>	<b>36</b> (11Tof + 14T)
block 2	50	95	<b>91</b>	<b>58</b> (22Tof + 14T)
<b>Grover<sub>5</sub></b>		<b>44 [16]</b>	152	<b>66</b> (27Tof + 12T)
block 1	58	108	<b>107</b>	<b>44</b> (19Tof + 6T)
block 2	27	46	<b>45</b>	<b>22</b> (8Tof + 6T)
<b>Hamming<sub>15</sub> (high)</b>		<b>787<sup>†</sup></b> (1010 [16])	<b>773</b>	<b>440</b> (173Tof + 2CS + 90T)
block 1	58	92	92	<b>52</b> (21Tof + 10T)
block 2	49	78	78	<b>44</b> (18Tof + 8T)
block 3	56	82	<b>81</b>	<b>50</b> (18Tof + 14T)
block 4	57	95	<b>94</b>	<b>55</b> (20Tof + 15T)
block 5	46	66	66	<b>40</b> (16Tof + 8T)
block 6	50	75	77	<b>45</b> (18Tof + 9T)
block 7	53	88	<b>86</b>	<b>50</b> (20Tof + 10T)
block 8	58	106	<b>100</b>	<b>53</b> (20Tof + 2CS + 9T)
block 9	59	105	<b>99</b>	<b>51</b> (22Tof + 7T)
<b>Hamming<sub>15</sub> (med)</b>		<b>156<sup>†</sup></b> (162 [16])	156	<b>78</b> (35Tof + 8T)
block 1	25	38	38	<b>20</b> (8Tof + 4T)
block 2	59	118	118	<b>58</b> (27Tof + 4T)
<b>Mod-Adder<sub>1024</sub></b>		<b>798<sup>†</sup></b> (978 [16])	<b>762</b>	<b>500</b> (141Tof + 15CS + 188T)
block 1	54	77	<b>75</b>	<b>42</b> (16Tof + 10T)
block 2	52	71	<b>70</b>	<b>47</b> (12Tof + 23T)
block 3	53	80	<b>76</b>	<b>48</b> (16Tof + 16T)
block 4	55	86	<b>77</b>	<b>47</b> (15Tof + 17T)
block 5	54	75	<b>73</b>	<b>53</b> (15Tof + 5CS + 13T)
block 6	52	84	<b>83</b>	<b>58</b> (13Tof + 5CS + 22T)
block 7	59	89	<b>87</b>	<b>60</b> (19Tof + 22T)
block 8	56	80	<b>73</b>	<b>54</b> (7Tof + 5CS + 30T)
block 9	56	96	<b>89</b>	<b>58</b> (17Tof + 24T)
block 10	53	60	<b>59</b>	<b>33</b> (11Tof + 11T)
<b>QCLA-Adder<sub>10</sub></b>		<b>116 [16]</b>	135	<b>94</b> (28Tof + 5CS + 28T)
block 1	37	53	53	<b>43</b> (12Tof + 19T)
block 2	48	83	<b>82</b>	<b>51</b> (16Tof + 5CS + 9T)
<b>QCLA-Mod<sub>7</sub></b>		<b>165 [16]</b>	199	<b>122</b> (43Tof + 36T)
block 1	50	95	95	<b>60</b> (21Tof + 18T)
block 2	59	107	<b>104</b>	<b>62</b> (22Tof + 18T)

**Table 3:** T-count achieved by different methods on a set of benchmark circuits, after splitting them into sub-circuits (blocks). AlphaTensor-Quantum finds good trade-offs between gadgets and T gates and outperforms the baseline methods for all circuits except Grover<sub>5</sub>. The T-count from AlphaTensor-Quantum is obtained by additively combining all sub-circuits. The baseline T-count for the sub-circuits is given by a combination of methods (see Appendix B). For the shaded rows, the baseline corresponds to the lowest between the best reported value in the literature and the sum of the T-count across sub-circuits (the symbol <sup>†</sup> indicates it is the latter case and also includes in parenthesis the best reported value in the literature, for completeness). The notation “ $a$ Tof+ $b$ CS + $c$ T” indicates  $a$  Toffoli gates,  $b$  CS gates, and  $c$  T gates. Bold font highlights results with strictly better T-count than the baselines.